BILINGUAL PUBLISHING CO.
Pioneer of Global Academics Since 1984

# Journal of Metallic Material Research

Volume 4 · Issue 2 · October 2021 | ISSN 2630-5135 (Online)

Volume 4 Issue 2 • October 2021 • ISSN 2630-5135 (Online)

# Journal of Metallic Material Research

**Editor-in-Chief**

Dr. Oleg Valentinovich

BILINGUAL PUBLISHING CO.
Pioneer of Global Academics Since 1984

BILINGUAL PUBLISHING CO.
Pioneer of Global Academics Since 1984

Volume 4 | Issue 2 | October 2021 | Page1-25
Journal of Metallic Material Research

# Contents

## Editorial



## Articles

BILINGUAL PUBLISHING CO.
Pioneer of Global Academics Since 1984

**Journal of Metallic Material Research**
https://ojs.bilpublishing.com/index.php/jmmr

ARTICLE

# Surface Tension of GaInSnBiZn Liquid High-entropy Alloy

**Shirong Zhu  Lu Liu  Qiaoli Lin***

State Key Laboratory of Advanced Processing and Recycling of Non-ferrous Metal, Lanzhou University of Technology, Lanzhou, 730050, China

ARTICLE INFO

*Article history*
Received: November 12 2021
Accepted: December 10 2021
Published Online: 15 December 2021

*Keywords*:
High-entropy alloy
Pendant-drop method
Thermodynamics
Formation entropy

ABSTRACT

As an emerging alloy material, high-entropy alloy has potential applications that distinguish it from traditional alloys due to its special physicochemical properties. In this work, a low melting point GaInSnBiZn high-entropy alloy was designed based on Miedema model, and its surface tension was measured by the continuous pendant-drop method. The results show that the intrinsic surface tension of GaInSnBiZn high-entropy alloy at 80 °C is 545±5 mN/m, and the surface tension of the liquid alloy is significantly reduced by the formation of surface oxide film. The surface tension of GaInSnBiZn high-entropy alloy was analyzed by using theoretical models (Guggenheim model, GSM (general solution) model and Butler model), and the thermodynamic characteristics of the surface tension formation were further verified by combining with thermodynamic calculations, among which the calculated results of Butler model were in good agreement with the experimental data. Meanwhile, it is found that the surface concentration of Bi in the alloy is much larger than the nominal concentration of its bulk phase, which contributes the most to the surface tension of the alloy, however, it contributes the least to the entropy of the alloy formation in combination with the Butler model.

## 1. Introduction

Surface tension is a fundamental physical property of liquid materials and its magnitude determines the conduct of many production processes, such as joining, electronic packaging, and forming [1,2]. On the other hand, high-entropy alloys, as an emerging multi-component alloy material, have shown impressive potential applications with their unique physicochemical properties under extreme conditions [3-6]. Therefore, mastering the surface/interfacial properties of liquid high-entropy alloys is of great research importance to expand their further applications.

For the measurement of surface tension of liquid metals, it mainly involves the general means such as the sessile-drop method, the pendant-drop method, the maximum bubble pressure method, and the droplet oscillation method. Each method has its own advantages and disadvantages, for

*Corresponding Author:
Qiaoli Lin,
State Key Laboratory of Advanced Processing and Recycling of Non-ferrous Metal, Lanzhou University of Technology, Lanzhou, 730050, China;
*Email: lqllinqiaoli@163.com*

DOI: https://doi.org/10.30564/jmmr.v4i2.4091

example, the sessile-drop and pendant-drop methods require a smaller amount of liquid compared to the maximum bubble pressure method, and the droplet oscillation method requires magnetic levitation or microgravity conditions and is much less accurate than the sessile-drop and pendant-drop methods [7-9]. In the case of liquid metals, the oxidizable nature of the surface (except for inert noble metals) can easily lead to small apparent values or even to surface tension values without any physical significance, regardless of the method used. For this reason, in most cases, surface tension measurements on liquid metals are generally performed under controlled atmospheres, such as high vacuum (ultra-high vacuum), inert atmospheres (argon or helium), or even reducing atmospheres (hydrogen), which makes the implementation of surface tension measurements extremely inconvenient. Once the oxide film is formed on the liquid metal surface, a fresh liquid metal surface can be obtained by forming a pendant drop by mechanical extrusion, which allows the original liquid metal surface oxide film to be removed. Since the formation of the oxide film on the liquid metal surface takes a certain amount of time, even at the fastest it takes at least 0.02 seconds [10]. The formation of hanging drops by continuous extrusion of the liquid metal and its capture using a high-speed camera makes it a possibility to measure the surface tension of liquid metals under the atmosphere. It is well known that the mixing Gibbs free energy ($G^{mix}=H^{mix}-TS^{mix}$) of high entropy alloys (HEA) is mainly derived from the contribution of mixing entropy to the formation of the alloy, so the mixing enthalpy of the alloy is as close to zero or positive as possible, and the more complex the component, the higher the entropy value ($S^{mix}=R\ln N$, where $R$ is the gas constant and $N$ is the number of alloy components). Meanwhile, the multi-component composition of high-entropy alloys poses difficulties for the theoretical prediction of surface tension, and the typical surface tension characteristics of high-entropy alloys cannot be reliably related to thermodynamic parameters.

In this work, a low melting point GaInSnBiZn high entropy alloy is designed based on the Miedema model. As a new low melting point liquid metal, it is expected to have potential applications in chip and thermal management devices and liquid metal printed circuits through the characterization of its thermal properties and the study of field phenomena and effects.

## 2. Alloy Design and Preparation

The mixing enthalpies of the binary alloys based on the Miedema model, as shown in Table 1, are positive except for the In-Sn and In-Bi binary systems, and both In-Sn and In-Bi mixing enthalpies are close to positive values. the binary phase diagram of In-Sn indicates the presence of solid solution without intermetallic compound formation; the binary phase diagram of the In-Bi system indicates the possible presence of both BiIn, $Bi_3In_5$ and $BiIn_2$ intermetallic compounds with melting points of 110 °C, 88.9 °C and 89.5 °C, respectively, where $BiIn_2$ has a mutual transformation with the solid solution of In containing Bi at 49 °C [11]. From the enthalpy of formation of ternary alloys, there is no ternary compound for alloy formation. Therefore, the GaInSnBiZn alloy mixed in equal proportions satisfies the thermodynamic conditions for the formation of a high entropy alloy.

The GaInSnBiZn high-entropy alloy was obtained from pure metal sheets with purity of Ga ≥ 99.999%, Bi ≥ 99.999%, In ≥ 99.999%, Sn ≥ 99.99%, and Zn ≥ 99.99%, respectively, which were cut and placed in corundum crucible and heated to 425 °C under high vacuum ($10^{-3}$ Pa) for half an hour, and then cooled rapidly. The GaInSnBiZn high-entropy alloy was further characterized by metallographic analysis (Keyence, VHX-900, Japan) to determine the microstructural characteristics and simultaneous thermal analysis (Netzsch, STA 449, Germany) to determine the melting point and possible phase transitions. The kinetic process of oxide film generation on liquid metal surfaces was characterized by laser (wavelength 632.8 nm) ellipsometry (Sentech, SE 400adv-PV, Germany).

**Table 1.** Mixing enthalpy and formation enthalpy of alloys in binary and ternary systems

| Binary systems | $\Delta H^{mix\quad i}_{in\,j\,or\,j\,in\,i}$, kJ/mol |
|---|---|
| Ga-In | 10.177, 11.983 |
| Ga-Sn | 3.239, 4.035 |
| Ga-Bi | 14.342, 20.011 |
| Ga-Zn | 0.064, 0.054 |
| In-Zn | 14.193, 10.117 |
| In-Sn | −1.415, −1.488 |
| In-Bi | −4.738, −5.582 |
| Sn-Bi | 4.808, 5.384 |
| Sn-Zn | 5.272, 3.578 |
| Bi-Zn | 22.764, 13.796 |
| Ternary systems | $\Delta H^{f}$, kJ/mol |
| Ga-In-Sn | 2.077 |
| Ga-In-Bi | 3.484 |
| Ga-In-Zn | 3.944 |
| Ga-Sn-Bi | 4.169 |
| Ga-Sn-Zn | 1.359 |
| Ga-Bi-Zn | 5.980 |
| In-Sn-Bi | 0.229 |
| In-Sn-Zn | 2.198 |
| In-Bi-Zn | 3.444 |
| Sn-Bi-Zn | 4.238 |

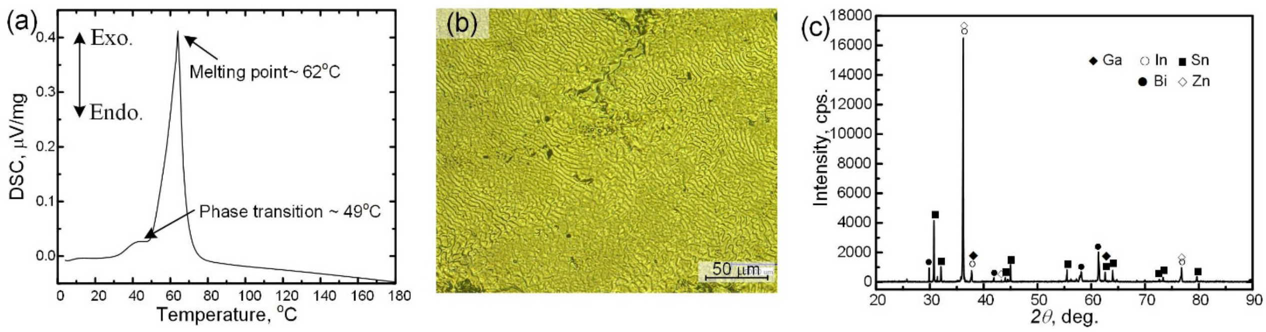


**Figure 1.** Physicochemical properties and microstructures of GaInSnBiZn high-entropy alloy
(a) DCS results; (b)Typical microstructures; (c) XRD spectrum

The GaInSnBiZn alloy after melting was ramped up to 180 °C at 5 °C/min for simultaneous thermal analysis. As shown in Figure 1a, an endothermic peak appeared at 49.6 °C, which according to the phase diagram corresponds to the temperature point at which the phase transition between $BiIn_2$ and In solid solution with Bi; an obvious endothermic peak appeared at 62.4 °C, which corresponds to the melting point of the alloy. The typical metallographic microstructures are shown in Figure 1b, with a relatively homogeneous microstructures and no segregation generation. The XRD pattern of the alloy after solidification (shown in Figure 1c), no obvious solid solution or intermetallic compounds could be identified after the formation of the alloy.

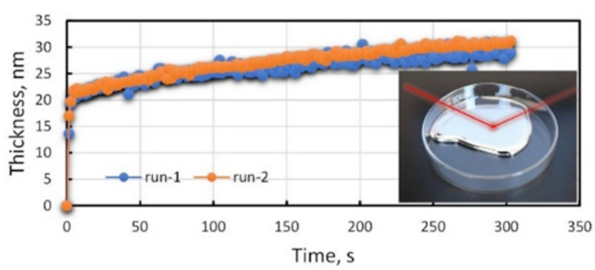


**Figure 2.** Variation of oxide film thickening with time of GaInSnBiZn high-entropy alloy

When the GaInSnBiZn alloy was melted at a constant temperature platform (constant temperature of 80 °C), the oxide film was scraped off with a ceramic sheet and the laser ellipsometer was applied, setting the laser incidence angle to 75°, and the complex refractive index and absorption coefficient were measured as 1.0422 and 6.4159, respectively. After being exposed to atmosphere for 5 min, the measured complex refractive index and absorption coefficient were 1.2644 and 6.1039, respectively. Based on this, after repeated in-situ measurements, the variations of oxide film thickening were obtained, is shown in Figure 2. The oxide film can be completely covered in about 2 s. Subsequently, the oxide film thickening shows a slow growth in logarithmic form with thickness variation between 20-30 nm, and even after 24 h, the oxide film thickness on the liquid metal surface is still about 40 nm, reflecting the good passivation effect of the oxide film. Based on the above results, the application of high-speed continuous extrusion to form hanging drops (at a rate of about 20 ms/drop), even under atmospheric atmosphere, is sufficient to obtain a clean, oxide film-free surface for measuring the intrinsic surface tension of liquid metals.

## 3. Surface Tension Measurement

The reliability of this method of measurement was first verified by recording continuous droplet squeeze drops by high-speed camera. The eutectic Ga-In alloy (E-GaIn, eutectic point of 16 °C, density 6.280 g/cm$^3$) was used for the study, and the outer diameter of the drop tube used was 0.46 mm. as shown in Figure 3a, the Young-Laplace curve matched well with the shape of the droplet profile, and the surface tension obtained was 623.1 mN/m (where the measurement error was (1.79-2.23) × $10^{-3}$ mN/m), which is in agreement with the literature [12]. E-GaIn alloys are oxidation-sensitive metals, and once a $Ga_2O_3$ oxide film is formed on the surface, it decreases the apparent surface tension of the droplet. As shown in Figure 3b, after the formation of static pendant-drop exposed to the atmosphere, the surface tension of the droplet surface subjected to the oxidation gradually decreases and shows an exponential decay form, which is obviously closely related to the oxygen concentration of the droplet surface, i.e., the surface tension gradually decreases with the increase of surface oxygen concentration.

According to the melting point of GaInSnBiZn alloy, a simultaneous heater was designed, and assembled for the drop tube and the sample stage, as shown in Figure 4. Under the condition of maintaining a constant temperature of 80 °C, the volume of the droplet was measured by the sessile-drop method, and the mass of the sessile-drop was obtained in combination with an analytical balance (accuracy of 0.0001 g), and the density of the liquid GaInSnBiZn alloy was calculated to be 6.8413-6.8416 g/cm$^3$. The surface tension of GaInSnBiZn alloy was also determined by the continuous pendant-drop method, which was 545±5 mN/m, as shown in Figure 5a. When the droplets were exposed to atmosphere for a few seconds, the droplet profile shape changed significantly, as shown in Figure 5b, and the surface tension decreased significantly to 252±20 mN/m. In the order of oxidizability of the alloy composition Zn>Ga>In>Sn>Bi, it is possible that the decrease in surface tension after oxidation is related to the formation of ZnO and $Ga_2O_3$.

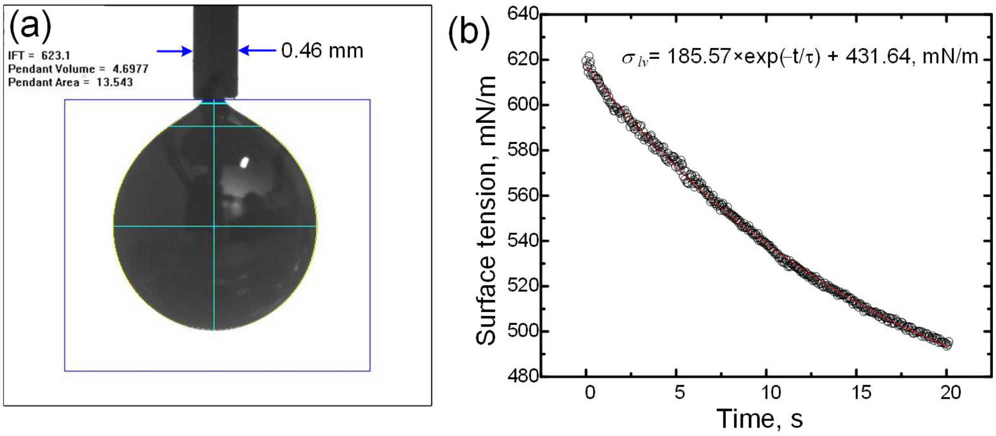


**Figure 3.** (a) Surface tension of E-GaIn alloy measured at 0.46 mm outside diameter of the drop tube; (b) Variation of surface tension with exposure time of liquid E-GaIn alloy

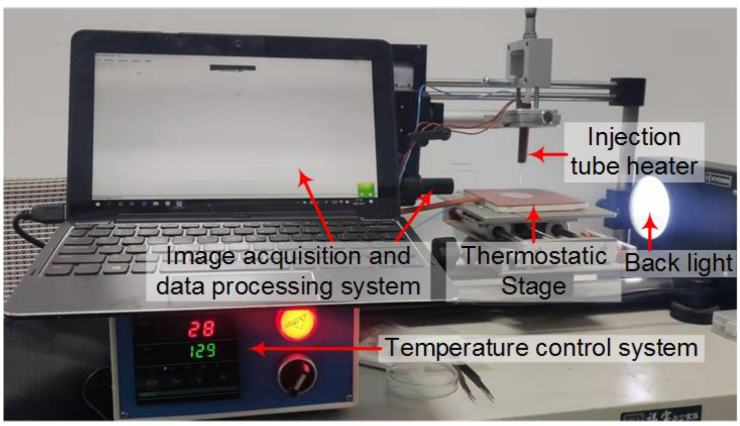


**Figure 4.** Surface tension measurement device after the introduction of heating and temperature control system

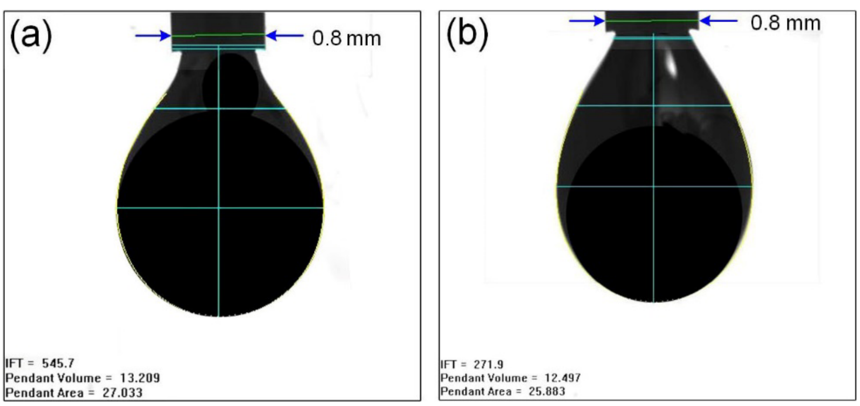


**Figure 5.** Surface tension of GaInSnBiZn alloy measured at 0.8 mm outside diameter of the drop tube.
(a) instantaneous snap of pendant-drop; (b) pendant-drop after exposure air for several seconds

## 4. Surface Tension Analysis of Multi-component Alloys

For an ideal solution, the surface tension can be expressed as,

$$\sigma^i = x_{Ga}\sigma_{Ga} + x_{In}\sigma_{In} + x_{Sn}\sigma_{Sn} + x_{Bi}\sigma_{Bi} + x_{Zn}\sigma_{Zn} \tag{1}$$

Where $\sigma^i$ is the surface tension under ideal solution conditions, and $x_i$ is the molar fraction of each component. Since the equal atomic proportions are mixed as shown in Table 2, $\sigma^i$ = 597.8 mN/m under ideal solution conditions, density $\rho^i$ is 7.341 g/cm$^3$, and molar mass $M^i$ is 115.522 g/mol.

Based on the assumption of high entropy alloy formation, all atoms are randomly distributed under ideal conditions, i.e., the solution formed is an ideal solution. Obviously, the measured data of surface tension and density indicate that the liquid GaInSnBiZn alloy is not an ideal solution, and the existence of local clusters or segregation within the liquid phase makes the apparent value of surface tension deviate from the ideal solution model.

**Table 2.** Surface tension ($\sigma_i$), density ($\rho$), molar mass ($M_i$) and molar area ($\Omega_i$) of pure metal at melting point

| | Ga* | In | Sn | Bi | Zn |
|---|---|---|---|---|---|
| $\sigma_i^0$, mN/m | 713 | 556 | 560 | 378 | 782 |
| $\rho_i$, g/cm$^3$ | 6.07 | 7.03 | 6.98 | 10.05 | 6.575 |
| $M_i$, g/mol | 69.72 | 114.8 | 118.7 | 209.0 | 65.39 |
| $\Omega_i$, m$^2$/mol | 4.74×10$^4$ | 5.78×10$^4$ | 5.91×10$^4$ | 7.09×10$^4$ | 4.04×10$^4$ |

*Ga is the surface tension and density at 80 °C

Currently, most of the theoretical models for surface tension of multivariate (quaternary or even quintuplet) alloys are predicted based on binary alloy system models, such as the Guggenheim model [13], the GSM (universal solution) model [14] and the Butler model [15].

The Guggenheim model [13] is expressed as,

$$e^{-(\frac{\sigma\Omega}{RT})} = \sum_{i=5}^{5} e^{-(\frac{\sigma_i\Omega_i}{RT})} \tag{2}$$

Where $\Omega_i$ is the molar area of a single component, can be calculated from $\Omega_i = fN_a^{1/3}V_i^{2/3}$, where f is a structure factor (equals 1.091), $N_a$ is Avogadro constant and $V_i$ is the molar volume ($V_i = M_i/\rho_i$). Substituting the data in Table 2 yields a surface tension of 440 mN/m, which is obviously far from the surface tension obtained from the actual measurement.

The Butler model [15] is expressed as,

$$\sigma = \sigma_i + \frac{RT}{\Omega_i}\ln\frac{c}{1+(c-1)x_i^b} \tag{3}$$

where $c = e^{-(\frac{\Omega_i(\sigma_2^0-\sigma_1^0)}{RT})}$.

**Table 3.** Surface tension and excess surface tension of binary alloys mixed at 1:1 atomic ratio

| Binary systems | Ideal solution, mN/m | Belton model, mN/m | $\sigma_{ij}^E$, mN/m |
|---|---|---|---|
| Ga-In | 635 | 592 | −43 |
| Ga-Sn | 637 | 595 | −42 |
| Ga-Bi | 546 | 414 | −132 |
| Ga-Zn | 748 | 739 | −9 |
| In-Zn | 669 | 597 | −72 |
| In-Sn | 558 | 558 | 0 |
| In-Bi | 467 | 409 | −58 |
| Sn-Bi | 469 | 409 | −60 |
| Sn-Zn | 671 | 600 | −71 |
| Bi-Zn | 580 | 417 | −163 |

The GSM model [14] can be expressed as,

$$\sigma^E = \frac{x_1x_2}{X_1X_2}\sigma_{1,2}^E + \frac{x_1x_3}{X_1X_3}\sigma_{1,3}^E + \frac{x_1x_4}{X_1X_4}\sigma_{1,4}^E + \frac{x_1x_5}{X_1X_5}\sigma_{1,5}^E + \frac{x_2x_3}{X_2X_3}\sigma_{2,3}^E + \frac{x_2x_4}{X_2X_4}\sigma_{2,4}^E + \frac{x_2x_5}{X_2X_5}\sigma_{2,5}^E + \frac{x_3x_4}{X_3X_4}\sigma_{3,4}^E + \frac{x_3x_5}{X_3X_5}\sigma_{3,5}^E + \frac{x_4x_5}{X_4X_5}\sigma_{4,5}^E \tag{4}$$

Where $\sigma^E$ is the excess surface tension, i.e., the partial surface tension that deviates from the ideal solution, $\sigma^E = \sigma - \sigma^i$. $x_i$ is the concentration of element $i$ in the five-element system, and $X_i$ is the concentration of element $i$ in the binary system. Since the alloy is mixed with equal atomic ratio, $x_i$ =0.2 and $X_i$ =0.5, $\sigma^E$ =−104 mN/m can be obtained from the data in Table 3, and the surface tension $\sigma$ predicted by the model is 493.8 mN/m, which again deviates from the measured value.

Nevertheless, the predictions of the above models indicate that the actual surface tension of GaInSnBiZn should have a negative deviation with respect to the ideal solution, i.e., the actual surface tension should be less than the surface tension obtained from the ideal solution model. Since the alloy is mixed with equal atomic ratios, the surface tension of the alloy is 533 mN/m by taking the average value of the surface obtained from the Belton model, so the Butler model (or Belton model) is closer to the measured value.

In addition, according to the Butler model, the concentration of elements on the surface can be expressed as,

$$x_i^s = x_i^b \exp\left[\frac{(\sigma-\sigma_i)\Omega_i - 0.17\Delta S_i^E T}{RT}\right] \tag{5}$$

In high entropy alloys, the free energy of alloy formation is mainly derived from the contribution of entropy, so the excess free energy of the bulk phase in the above equation is replaced by $\Delta S_i^E T$. It can be concluded that the larger the contribution of each element to the excess entropy, the smaller its concentration at the surface and the smaller its contribution to the surface tension. The surface tension of the alloy is positive compared to the surface tension of the pure substance of each element, only the excess surface tension of the Bi element, where $x^s_{Ga} + x^s_{In} + x^s_{Sn} + x^s_{Bi} + x^s_{Zn} = 1$. The surface concentration of all the elements except Bi is less than the nominal concentration of the bulk phase 0.2, which means that the surface concentration of Bi is much larger than the nominal concentration of the bulk phase ($x^s_{Bi} > 0.2$), and thus the contribution of Bi to the entropy of alloy formation is minimal.

## 5. Conclusions

(1) The intrinsic surface tension of GaInSnBiZn high-entropy alloy at 80 °C was determined by the continuous pendant-drop method as 545±5 mN/m. The surface tension of the alloy decreased significantly with the formation of the surface oxide film.

(2) The Guggenheim model, GSM model, and Butler model were applied to calculate the surface tension of GaInSnBiZn high-entropy alloy, among which the calculation results obtained from the Butler model are in good agreement with the experimental data. Combined with the Butler model, the surface concentration of Bi is much higher than the other components and contributes the most to the surface tension, however, it contributes the least to the entropy of alloy formation.

## Credit Authorship Contribution Statement

Shirong Zhu: Methodology, Writing, original draft. Lu Liu: Data analysis, Editing. Qiaoli Lin: Supervision, Work idea, Revision.

## Declaration of Competing Interest

The authors declare that they have no known competing financial interests or personal relationships that could have appeared to influence the work reported in this paper.

## Funding

This work is supported by National Natural Science Foundation of China (No. 52165044).

## Conflict of Interest

No conflict of interest exists to declare.

## References

[1] Wang, X., Guo, R., Liu, J., 2019. Liquid metal based soft robotics: materials, designs, and applications. Advanced Materials Technologies. 4, 1800549.

[2] Zhao, X., Xu, S., Liu, J., 2017. Surface tension of liquid metal: role, mechanism and application. Frontiers in Energy. 11, 535-567.

[3] Joo, S.H., Kato, H., Jang, M.J., Moon, J., Kim, E.B., Hong, S.J., Kim, H.S., 2017. Structure and properties of ultrafine-grained CoCrFeMnNi high-entropy alloys produced by mechanical alloying and spark plasma sintering. Journal of Alloys and Compounds. 698, 591-604.

[4] Zhang, Y., Zuo, T.T., Tang, Z., Gao, M.C., Dahmen, K.A., Liaw, P.K., Lu, Z.P., 2014. Microstructures and properties of high-entropy alloys. Progress in Materials Science. 61, 1-93.

[5] Ye, Y.X., Liu, C.Z., Wang, H., Nieh, T.G., 2018. Friction and wear behavior of a single-phase equiatomic TiZrHfNb high-entropy alloy studied using a nanoscratch technique. Acta Materialia. 147, 78-89.

[6] Yan, X., Zhang, Y., 2020. Functional properties and promising applications of high entropy alloys. Scripta Materialia. 187, 188-193.

[7] Fujii, H., Matsumoto, T., Nogi, K., 2000. Analysis of surface oscillation of droplet under microgravity for the determination of its surface tension. Acta Materialia. 48, 2933-2939.

[8] Przyborowski, M., Hibiya, T., Eguchi, M., Egry, I., 1995. Surface tension measurement of molten silicon by the oscillating drop method using electromagnetic levitation. Journal of Crystal Growth. 151, 60-65.

[9] Iida, T., Guthrie, R., 1988. The Physical Properties of Liquid Metals. UK: Oxford University Press.

[10] Ding, Y., Zeng, M., Fu, L., 2020. Surface chemistry of gallium-based liquid metals. Matter. 3, 1477-1506.

[11] Cui, Y., Ishihara, S., Liu, X., Shirong, Ohnuma, I., Kainuma, R., Ohtani, H., Ishida, K., 2002. Thermodynamic calculation of phase diagram in the Bi-In-Sb ternary system. Materials Transactions. 43, 1879-1886.

[12] Ren, L., Xu, X., Du, Y., Kalantar-Zadeh, K., Dou, S.X., 2020. Liquid metals and their hybrids as stimulus–responsive smart materials. Materials Today. 34, 92-114.

[13] Guggenheim, E.A., 1945. Statistical thermodynamics of the surface of a regular solution. Transactions of the Faraday Society. 41, 150-156.

[14] Yan, L., Zheng, S., Ding, G., Xu, G., Qiao, Z., 2007. Surface tension calculation of the Sn–Ga–In ternary alloy. Calphad. 31(1), 112-119.

[15] M'chaar, R., Sabbar, A., El Moudane, M., Ouerfelli, N., 2020. A survey of surface tension, molar volume and density for Sn–Ag–Cu–Bi–Sb quinary alloys as lead-free solders. Philosophical Magazine. 100, 1415-1438.

Journal of Metallic Material Research
https://ojs.bilpublishing.com/index.php/jmmr

ARTICLE

# Investigation and Mathematical Modelling of Optimized Cutting Parameters for Surface Roughness of EN-8 Alloy Steel

**Amit Saraswat Dipak Kumar***

Mechanical Engineering Department, RKGIT Ghaziabad, 201003, India

ARTICLE INFO

*Article history*
Received: 13 November 13 2021
Accepted: 13 December 13 2021
Published Online: 20 December 2021

*Keywords*:
Cutting parameters
Surface roughness
EN-8 steel
Optimization
Modelling

ABSTRACT

The work done in this work deals with the efficacy of cutting parameters on surface of EN-8 alloy steel. For knowing the optimal effects of cutting parameters response surface methodology was practiced subjected to central composite design matrix. The motive was to introduce an interaction among input parameters, i.e., cutting speed, feed and depth of cut and output parameter, surface roughness. For this, second order response surface model was modeled. The foreseen values obtained were found to be fairly close to observed values, showed that the model could be practiced to forecast the surface roughness on EN-8 within the range of parameter studied. Contours and 3-D plots are generated to forecast the value of surface roughness. It was revealed that surface roughness decreases with increases in cutting speed and it increases with feed. However, there were found negligible or almost no implication of depth of cut on surface roughness whereas feed rate affected the surface roughness most. For lower surface roughness, the optimum values of each one were also evaluated.

## 1. Introduction

Nowadays each and every company want to get the maximum return with retaining good quality that is possible through selection of optimum parameters and understanding of modern trends with prior analysis. These demands are still attracting the attention of researchers towards the work on process parameters and searching the optimal parameter framework which is used for attaining the process effectively. The process parameter also comprises the internal and external basics of the process. To obtain the robust process with error free it is needed to enhance the performance of cutting process, it is imperative to optimize the process parameters. In the view of significant of machining process, critical reviews that were attained by the various researchers on different materials are discussed.

Sharma et al. [1] conducted experiment on AISI 52100 steel using a carbide-coated tool in turning operations using different cutting parameters. The surface roughness was also measured subjected to the effect of cutting parameters such as approach angle, speed, feed rate and

*Corresponding Author:
Dipak Kumar,
Mechanical Engineering Department, RKGIT Ghaziabad, 201003, India;
*Email: dipakmnnit@gmail.com*

DOI: https://doi.org/10.30564/jmmr.v4i2.4094

depth of cut. They concluded that the surface roughness increased with increasing feed rate. The speed had somewhat effect on the roughness, and the surface roughness decreased slightly with increasing approach angle and depth of cut.

Fnides et al. [2] worked on grade X38CrMoV5-1 steel, hot work steel and they found good strength to high temperature and its ability for polishing empower it to answer the most harsh case in hot dying and moulds under pressure.

Selvaraj and Mohan [3] reported the work on dry turning of AISI 304 Austenitic Stainless Steel (ASS). For this, they planned design of experiments based on Taguchi's technique and eventually the confirmation tests were conducted to match the predicted with the experimental ones for its proficiency in the examination of surface roughness.

Kuram et al. [4] used three distinct vegetable-based cutting fluids for knowing the thrust force and surface roughness during drilling of AISI 304 austenitic stainless steel with HSSE tool. They investigated usefulness of vegetable cutting oils to mitigate thrust force and improving surface finish at all machining conditions.

Selvaraj and Chandramohan [5] carried out work on dry turning of cast duplex stainless steels (ASTM A 995 Grade 4A and ASTM A 995 Grade 5A) using TiC and TiCN coated cemented carbide cutting tools. They found reversible relationship trends between rising cutting speed and surface roughness up to some point. It was obtained usefulness of alpha fiber in the austenite phase of 4A work piece material in surface finishing. In addition to this, surface finish of grade 4A was found to be better than other material.

Hatem [6] designed of experiment to obtain surface quality of the turning and model of surface roughness with the cutting speed, feed rate for different materials at constant depth of cut (0.5mm). They also tried to understand the actual difficulties comes into governing the finish of machined surfaces while adjusting the process parameters to get a surface finish.

Sastry et al. [7] produced aluminum and resin work pieces by machine-turning, and their surface quality and metal removal rate were analyzed along with potential effects of variables such as cutting speed, feed and depth of cut onto two different work pieces. They also modelled using Response Surface Method (central composite design) and validated the adequacy of the models.

Ficici et al. [8] studied the optimal cutting condition for drilling operation of stainless steel by varying cutting parameters through the Taguchi optimization technique and they statistical showed the results (at a 99.5% confidence level) that the drill modification condition (A), cutting speed (B) and feed rate (C) influence the surface roughness in the drilling process by 74.25%, 13.72%, and 6.25%, respectively. The interaction of $A$x$B$ had a much higher significant effect at 4.50% while interactions of $A$xC and $B$x$C$ had no significant effect on the surface roughness. Deviations between actual and predicted S/N ratios for the surface roughness were found eligibly small with 99.5% and 90% confidence levels respectively.

Korat and Agarwal [9] studied EN24 material in CNC turning for knowing the consequence of the process parameters viz. coolant condition, cutting speed, feed, depth of cut, nose radius, on response characteristics viz. material removal rate, surface roughness. It was shown that ANOVA (S/N Data) results shows the nose radius, feed rate, depth of cut, cutting speed and coolant condition affects the surface roughness by 65.38 %, 25.15 %, 3.06 %, 1.41 % and 0.09 % respectively.

Bhateja et al. [10] showed the effect of cutting parameters on EN-24 alloy steel and least roughness value for TNMG in the first step of step turning, second step of step turning, third step of turning. Thus, from the examination, it was concluded that the optimality of TNMG is known reason being the constancy from step 2, as well as lesser that Ra value of uncoated and coated step 3 (turning).

Ali et al. [11] presented a FEM model for predicting surface roughness for the face milling process in dry conditions and were found satisfactory results between predicted and calculated ones. It was concluded that FEM as beneficial tool for not only predict the value of feed cutting force to control the surface roughness rather than conducting experiments but lead to reduced machining time as well the manufacturing cost also.

Vipindas [12] applied Taguchi method for knowing the surface quality of Al6061 in turning operation and found feed as significant factor.

Gandhi [13] was employed principal component analysis (PCA) to eliminate response correlation and convert into uncorrelated quality indices called principal components and was confirmed better methodology for reducing the number of response variables.

Tulsiramarao [14] reported on the work of surface finishing of mild steel and alloy steel work pieces and obtained minimum surface roughness at 1600 rpm spindle speed, 0.1 mm depth of cut and 500 inch per min of feed rate.

Das et al. [15] studied on machining of hardened AISI4340 steel with multi-layered coated carbide insert using full factorial design of experiments (DOE) on turning and, determined the best combination of machining parameters and found feed as the most significant parameter followed by cutting speed. However, depth of cut did impact the surface roughness but at least.

Sahijpaul and Singh [16] used custom design approach through JMP statistical software and was found to be lower surface roughness of EN-8 with decrease in cutting fluid concentration.

Patel et al. [17] found that for surface roughness the most significant parameters are speed, feed and nose radius as the most significant parameters while depth of cut (DOC) as the least significant parameter for roughness and, for material removal rate (MRR); DOC, feed and speed was observed as most significant and nose radius as the least.

Begic-Hajdarevic et al. [18] investigated that the better surface roughness could be achieved in high-speed milling of hardened tool steel during up-cut and down-cut process but with severity of tool wear.

Sarıkaya and Güllü [19] used AISI 1050 steel for turning machining using design of experiments and then it was modelled mathematically for surface roughness, namely Ra and Rz, through response surface methodology (RSM). The results indicated feed rate as the most influenced parameters on the surface roughness.

Kumar et al. [20] used Al-4.5Cu/TiC metal matrix composites for knowing the dry turning characteristics and their results indicated significant lower formation of BUE at larger value of cutting speed and vice-versa. The length of chip and the number of chip curls increased with an increase in cutting speed at given feed rate and depth of cut. At the same machining condition, C-type chips was changed to segmental type chip with the addition of weight percentage of reinforcement.

From the literature review, it was discovered from aforesaid that surface roughness and machining efficiency are foremost intentions but work on modelling and optimization were found very few for EN 8 Steel in CNC Turning by the use of different cutting parameter [21-26]. It was noted that the effect on surface roughness of work piece material by the specifying varying process parameters by employing empirical approach have not been yet explored, so it remains still the matter of attraction to work in the area of optimization of cutting parameters of EN 8 Alloy steel in CNC Turning.

The purpose of this research is to explore the systematic procedure of design of experiment & response surface methodology & hence to get optimum value of cutting parameter for CNC lathe machine to get the desired value of surface roughness for EN-8 steel.

## 2. Experimental Details

### 2.1 Material Detail

In this study EN-8 alloy steel is used, can be seen in Table 1. In this experiment carbide insert (DNMG 150608) as a cutting tool material made by Sandvik Coromant Limited was used. Dimension of tool was 15 mm × 0.6 mm × 0.8 mm and, dimension of tool holder as per ISO was DDJNL 20 × 20 K 15 where, D is clamping system, D is insert shape (55° Diamond shape), J is approach angle, N is clearance angle, L is left hand, K is tool length(152.4 mm) and 15 is insert edge length, respectively. The approach angle of the tool holder was 93° and 20×20 is taken as tool height × tool width. Typical turning, thread cutting and parting tools used in CNC Lathe used for current work is referred in Figure 1. And, photography of material samples is shown in Figure 2.

**Table 1.** Chemical Composition of EN-8 Steel.

| Elements | C | Mn | Si | Cr | Mo | Others | Fe |
|---|---|---|---|---|---|---|---|
| Wt.(%) | 0.399 | 0.643 | 0.175 | 0.013 | 0.002 | Balance | 98.653 |

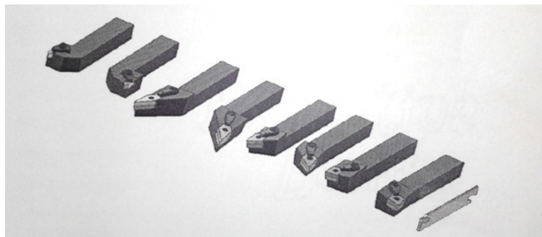

**Figure 1.** Typical Turning, Thread Cutting and Parting Tools used in CNC Lathe.

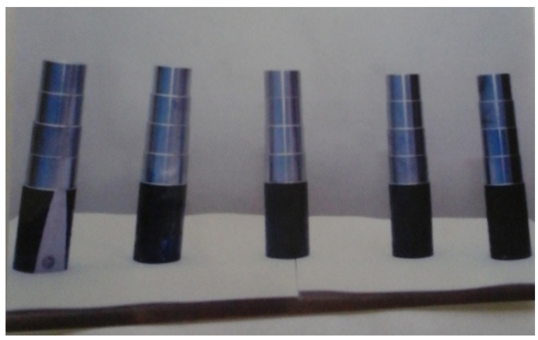

**Figure 2.** Photographic view of Test Specimens

### 2.1.1 Machining Details

The experiment was performed on CNC lathe machine, Make of HMT- STALLION-100 SU, can be seen in Figure 3. The STALLION-100 SU turning centre is devised to execute a various machining processes such as straight, taper turning, drilling, boring and contouring with linear and circular interpolation, internal and external threading (Parallel or taper) etc. The machine is appropriate for chucking and bar types of work pieces, also. CNC machine tool (machining and turning centres) is advanced type of numerically controlled machine tools used to fabricate a form of complex parts.

**Figure 3.** Pictorial view of STALLION 100 SU.

The feed drive for the saddle (Z-axis) and the feed drive for the cross slide (X-axis) are by AC servomotors, which are coupled with ball screw by bellow coupling. The standard rapid traverse rates for both Z and X-axes are 18000 mm/min. The standard turret has 8 tooling stations with wedge lock system. Tailstock system with MT-3 taper and live centre is provided on an auxiliary bed to increase the prospects of the machine without disturbing the distinctive features. The tailstock unit is flexible to the auxiliary bed or different work piece lengths.

### 2.1.2 Cutting Parameters Details

The major operating parameters affects the quality of surface finish in turning are the cutting speed (V), Feed rate (fr) Depth of cut (d) and Tool nose radius (r). For all metal cutting processes, "speed and feed" are imperative parameters. To narrate these parameters, it can be seen the Figure 4 showing the important geometry of fundamental machining parameters.

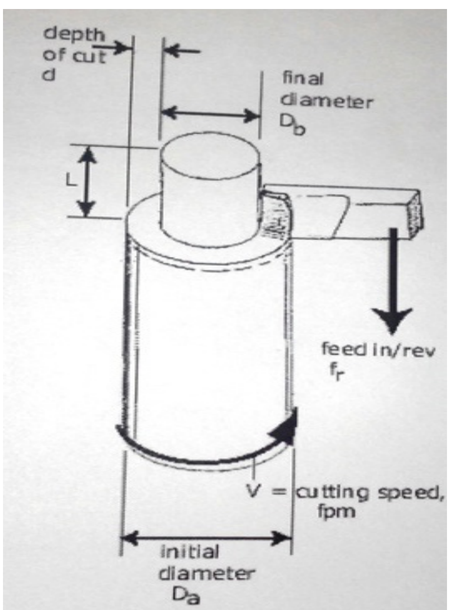


**Figure 4.** Geometry of Fundamental Machining Parameters.

For finishing operations, the rate of advance will be obsessed with the identified surface roughness for the finished product. The depth of cut will count on the particularized accuracy. The machining parameter, their range and levels used for experiment work are shown in Table 2.

### 2.2 Selection of Methods

In this we select the factors which affect the surface finish most. The factor in an experiment may be either quantitative or qualitative. If they are quantities, thought should be given as to how this factor is to be controlled at the desired value & the number of levels at which runs are to be constructed. These levels may be designated specifically or selected at random from the set of all achievable factor levels.

In choosing a response or depended variables, we must be assured that the response to be measured really provide the information about the problem under study. In this study response is surface roughness taken.

This step is of primary importance in the experimental process. It must be determined the difference in the true response the wish to detect & magnitude of the risk they are willing to tolerate so that an appropriate sample size may be chosen. We also determine the order in which the data will be collected. It is always necessary to maintain a balance between statistical accuracy & cost. A cost mathematical model for the experiment must be proposed, so that a statistical analysis of the data may be performed. We used central composite design which is very good for the analysis of second order equation.

### Response Surface Methodology

Its idea can be to improve the response or to figure out the underlying mechanism. If the input factor is assessable and there are only scarce where response surface methodology becomes an efficacious tool for studying this relationship. A sequential experimentation tactics is considered, which eases a productive search of the input factor space by using a first order experiment followed by a second-order experiment. Evaluation of a second-order experiment could be executed by supposing the response surface relationship with a fitted second-order regression models to be efficiently estimated are considered which is based on central composite designs. A central composite design for two variables is referred to as, can be shown in Figure 5. The design may be sub divided into three parts. Components of central composite design (CCD) used is shown in Table 3. Design for k = 3, 4, 5, 6 Note That with 5 and 6x-vaiables, the size of the experiment is reduced by using a half-replicate of the $2^k$ factorial. With a half-replicate, α becomes $2^{(k-1)/4}$. Experimental planned data based on CCD for test run can be shown in Table 4 and, their actual corresponding run data are referred in Table 5 and Table 6.

**Table 2.** Machining Parameter Ranges and Their Levels.

| S. No. | Parameter | Unit | Symbol | Range | Levels | | | | |
|---|---|---|---|---|---|---|---|---|---|
| | | | | | −1.68 | −1 | 0 | 1 | 1.68 |
| 1. | Cutting Speed | m/min | A | 110.5 to 225.5 | 110.5 | 139.25 | 168.0 | 196.75 | 225.5 |
| 2. | Feed | mm/rev | B | 0.04 to 0.2 | 0.04 | 0.08 | 0.12 | 0.16 | 0.2 |
| 3. | Depth of Cut | mm | C | 0.2 to 1.0 | 0.2 | 0.4 | 0.6 | 0.8 | 1.0 |
| 4. | Nose Radius | mm | D | 0.8 | 0.8 | 0.8 | 0.8 | 0.8 | 0.8 |

**Table 3.** Components of Central Composite Design.

| Number of points | | | | | |
|---|---|---|---|---|---|
| No. of x-variable k | $2^k$ Factorial | Axial | Center | Total N | Value of α |
| 3 | 8 | 6 | 6 | 20 | 1.682 |
| 4 | 16 | 8 | 6 | 30 | 2.000 |
| 5 | 16 | 10 | 6 | 32 | 2.000 |
| 6 | 32 | 12 | 6 | 53 | 2.378 |

**Table 4.** Treatment Combination for (Three variable-five level) Experiment coded form.

| **Run** | **Factor 1 A: Cutting speed (m/min)** | **Factor 2 B:Feed (mm/rev)** | **Factor 3 C: Depth of cut (mm)** |
|---|---|---|---|
| 1 | −1 | 1 | 1 |
| 2 | 1 | 1 | −1 |
| 3 | −1.68 | 0 | 0 |
| 4 | −1 | −1 | 1 |
| 5 | 0 | −1.68 | 0 |
| 6 | −1 | 1 | −1 |
| 7 | 0 | 0 | 0 |
| 8 | 0 | 0 | 0 |
| 9 | 1.68 | 0 | 0 |
| 10 | 1 | 1 | 1 |
| 11 | 0 | 1.68 | 0 |
| 12 | 0 | 0 | −1.68 |
| 13 | 0 | 0 | 0 |
| 14 | 0 | 0 | 0 |
| 15 | 0 | 0 | 0 |
| 16 | 0 | 0 | 1.68 |
| 17 | 0 | 0 | 0 |
| 18 | −1 | −1 | −1 |
| 19 | 1 | −1 | 1 |
| 20 | 1 | −1 | −1 |

**Table 5.** Treatment Combination in terms of Actual Factor.

| **Run** | **Factor 1 A: Cutting speed m/min** | **Cutting speed (N) rpm** | **Factor 2 B: Feed mm/rev** | **Factor 3 C: Depth of cut mm** |
|---|---|---|---|---|
| 1 | 139.25 | 1458 | 0.16 | 0.8 |
| 2 | 196.75 | 2116 | 0.16 | 0.4 |
| 3 | 110.5 | 1239 | 0.12 | 0.6 |
| 4 | 139.25 | 1654 | 0.08 | 0.8 |
| 5 | 168.0 | 1737 | 0.04 | 0.6 |
| 6 | 139.25 | 1478 | 0.16 | 0.4 |
| 7 | 168.0 | 1857 | 0.12 | 0.6 |
| 8 | 168.0 | 1938 | 0.12 | 0.6 |
| 9 | 225.5 | 2331 | 0.12 | 0.6 |
| 10 | 196.75 | 2145 | 0.16 | 0.8 |
| 11 | 168.0 | 1910 | 0.2 | 0.6 |
| 12 | 168.0 | 1938 | 0.12 | 0.2 |
| 13 | 168.0 | 1737 | 0.12 | 0.6 |
| 14 | 168.0 | 1807 | 0.12 | 0.6 |
| 15 | 168.0 | 1883 | 0.12 | 0.6 |
| 16 | 168.0 | 2026 | 0.12 | 1.0 |
| 17 | 168.0 | 1737 | 0.12 | 0.6 |
| 18 | 139.25 | 1478 | 0.08 | 0.4 |
| 19 | 196.75 | 2206 | 0.08 | 0.8 |
| 20 | 196.75 | 2270 | 0.08 | 0.4 |

**Table 6.** Experimental Observations.

| Run | Factor 1 A: Cutting speed m/min | Factor 2 B: Feed rate mm | Factor 3 C: Depth of cut mm | Response Surface Roughness |
|---|---|---|---|---|
| 1 | −1.00 | 1.00 | 1.00 | 1.56 |
| 2 | 1.00 | 1.00 | −1.00 | 1.58 |
| 3 | −1.68 | 0.00 | 0.00 | 1.47 |
| 4 | −1.00 | −1.00 | 1.00 | 0.87 |
| 5 | 0.00 | −1.68 | 0.00 | 2.02 |
| 6 | −1.00 | 1.00 | −1.00 | 1.78 |
| 7 | 0.00 | 0.00 | 0.00 | 0.98 |
| 8 | 0.00 | 0.00 | 0.00 | 1.07 |
| 9 | 1.68 | 0.00 | 0.00 | 1.21 |
| 10 | 1.00 | 1.00 | 1.00 | 1.61 |
| 11 | 0.00 | 1.68 | 0.00 | 2.01 |
| 12 | 0.00 | 0.00 | −1.68 | 1.6 |
| 13 | 0.00 | 0.00 | 0.00 | 1.05 |
| 14 | 0.00 | 0.00 | 0.00 | 1.11 |
| 15 | 0.00 | 0.00 | 0.00 | 1.115 |
| 16 | 0.00 | 0.00 | 1.68 | 1.116 |
| 17 | 0.00 | 0.00 | 0.00 | 0.58 |
| 18 | −1.00 | −1.00 | −1.00 | 2.54 |
| 19 | 1.00 | −1.00 | 1.00 | 0.66 |
| 20 | 1.00 | −1.00 | −1.00 | 0.7 |

## 2.3 Mathematical Modelling

Once the experimental design become final, the subsequent step is to fit the given data in mathematical model using regression analysis. Most of the engineering problems involve more than one variable. For example, surface roughness in the machining depends upon the feed, speed, depth of cut, nose radius, tool material etc. The general equation of fitting the second order model is

$$Y = \beta_0 + \beta_1 X_1 + \beta_2 X_2 + \beta_{12} X_1 X_2 + \beta_{11} X_1^2 + \ldots\ldots + e_u;$$

where β is called regression coefficients.

## Surface roughness measurement

In this study, direct method measurement method is used i.e., stylus type to measure the surface roughness of the specimen. The surface roughness meter used in our experiments is manufactured by MITUYOYO-JAPAN, make of JIS'94.

## 3. Results

First of it was drawn the ANOVA table to examine the good competence of the model. ANOVA Table is shown in Table 7 the calculation is done at 95% confidence level. In Prob>F column the values which are less than 0.05, are significant. In this case A, C, AB, AC are considerable model terms. It means that these terms influence the model to a great extent. Also, the lack of fit test is not significant. It means that these factors are adequately explaining the behavior of surface roughness.

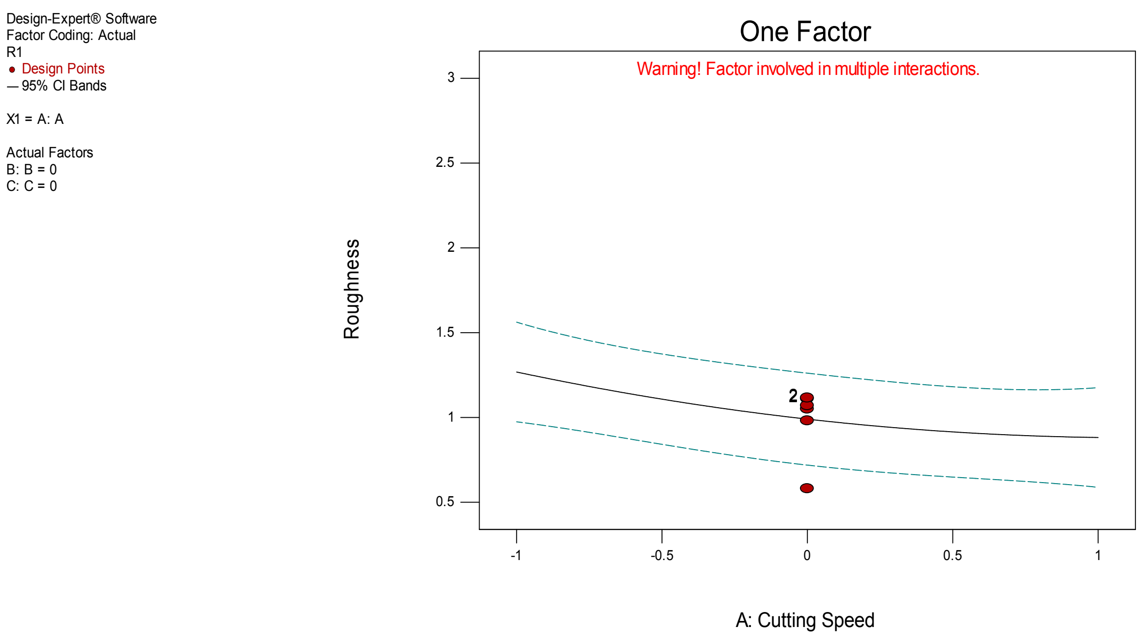


**Figure 5.** Surface Roughness vs Cutting Speed

**Table 7.** Analysis of Variance (ANOVA) Test for Surface Roughness.

| Source | Sum of Square | DOF | Mean Square | F value | P-value Prob>F | |
|---|---|---|---|---|---|---|
| Model | 4.04 | 9 | 0.45 | 5.05 | 0.0092 | significant |
| A-cutting speed | 0.51 | 1 | 0.51 | 5.72 | 0.0378 | |
| B-feed rate | 0.22 | 1 | 0.22 | 2.50 | 0.1449 | |
| C-depth of cut | 0.54 | 1 | 0.54 | 6.06 | 0.0336 | |
| AB | 0.45 | 1 | 0.45 | 5.07 | 0.0480 | |
| AC | 0.44 | 1 | 0.44 | 4.97 | 0.0500 | |
| BC | 0.29 | 1 | 0.29 | 3.25 | 0.1018 | |
| Residual | 0.89 | 10 | 0.089 | | | |
| Lack of Fit | 0.68 | 5 | 0.14 | 3.28 | 0.1093 | Not significant |
| Pure Error | 0.21 | 5 | 0.042 | | | |

## 3.1 Model Formation

The model has been formed with the help of software Design Expert's Version 9.0.2. The second order model given by the software is given below.

Surface roughness =

| | |
|---|---|
| +0.99043 | |
| -0.19311 | *cutting speed |
| +0.12764 | * feed rate |
| -0.19873 | * depth of cut |
| +0.23750 | * cutting speed * feed rate |
| +0.23500 | * cutting speed * depth of cut |
| +0.19000 | * feed rate * depth of cut |

### 3.1.1 Surface Roughness vs Cutting Speed

It is unambiguous from the Figure 5 that with increase in cutting speed, the value of surface roughness decreases that is the surface becoming smooth. The reason is that at low cutting speed, the cutting forces are high & hence the work material take up a new shape, i.e., a tougher built-up edge. Owing to rise in temperature it was found to be decrease in frictional stress occurring on the rake face with the higher cutting speed and cutting forces which may be reason to shape up the form of build edge but with less strength. Combination of these two effects were found valuable for surface finish. It was also noted that at relatively small cutting, temperature could not rise as per required that may cause for the formation of the built-up edges. On the other side, it was also noted that if the cutting speed further increases, the cutting become again progressively favour for shaping the built-up edge. In the end, at sufficiently high speed, the built edge fade totally & surface finish become insensitive of cutting speed.

### 3.1.2 Surface Roughness vs Feed Rate

As is vivid in Figure 6 with the increase in the value of feed, the surface roughness value increases drastically, at low feed rate, the fracture takes place which is very few when it was compared with high feed. With very small crevice in surface, it consistently ushers to roughness on surface fewer and vice versa. In addition to this, increase in feed assisted to increases in roughness which causes ultimately increased in forces and chattering phenomenon. This behavior caused for improper machining with faster traverse. It has also proved that [27] that $h = f^2/8r$, where, h, is peak to valley height, r is tool nose radius, and f is feed.

### 3.1.3 Surface Roughness vs Depth of Cut

As shown in Figure 7 initially with the increase in value of depth of cut there is very slight Decrease in surface roughness and on further increase there is very slight decrease in surface roughness. With the increase in depth of cut it was observed mounting in normal pressure which subsequently into seizure on the rake face and also assist in the shaping as the built-up edge [28,29]. Figure 8 shows the actual vs predicted data. This graph represents the differences between the actual values and the values that are predicted by the model. $R^2$ is the squared correlation of actual and predicted values and, as such, contains all the data that have been used for model estimation to judge the model's predictive power, it represents a measure of in-sample predictive power. Figure 9 shows the run vs

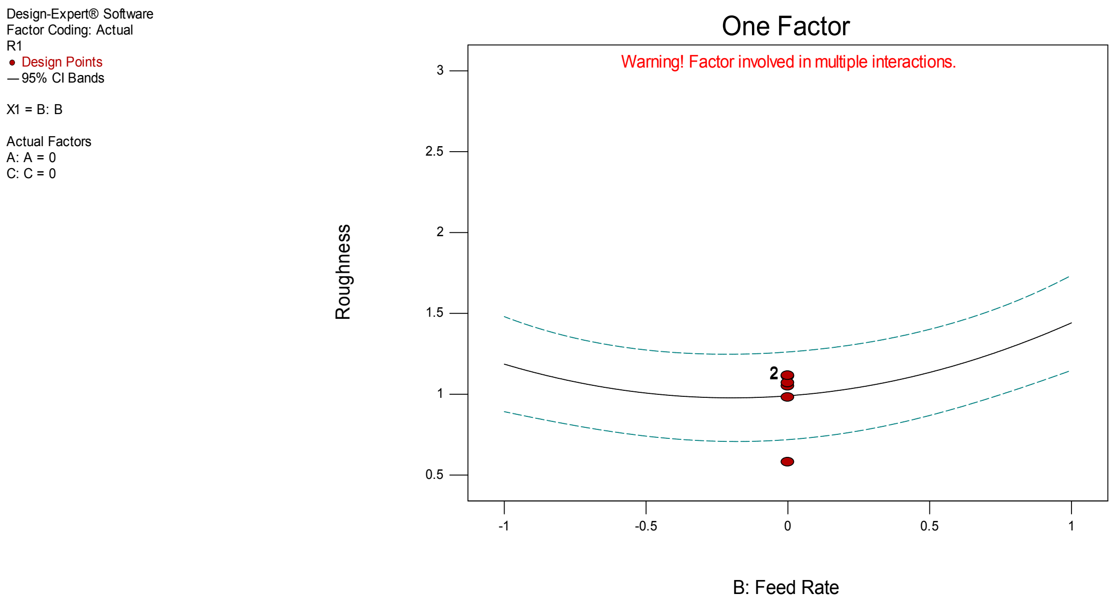


**Figure 6.** Surface Roughness vs Feed rate.

residuals which represents the residuals in each run. Figure 10 shows the contours in 3 d surfaces where contours along with three dimensional surfaces are shown in Figure 10, 11 and 12 with the help of these contours, the value of response can be calculated, can be seen in Table 8, at any point in the designated region. Figure 10 shows relationship between response surface between feed rate and cutting speed where the third parameter depth of cut kept constant at the middle value. Figure 11 shows response surface between the depth of cut and cutting speed where the third parameter feed rate kept constant at the middle value. Figure 12 shows relationship between response surface between the feed rate and depth of cut where the third parameter cutting speed kept constant at the middle value.

**Table 8.** Optimization Results.

| No. | Cutting speed | Feed rate | Depth of cut | Surface Roughness |
|---|---|---|---|---|
| 1 | 196.75 | 0.08 | 0.8 | 0.778 |
| 2 | 196.75 | 0.08 | 0.4 | 1.085 |
| 3 | 196.75 | 0.16 | 0.4 | 1.436 |
| 4 | 139.25 | 0.16 | 0.4 | 1.817 |
| 5 | 139.25 | 0.08 | 0.4 | 2.417 |

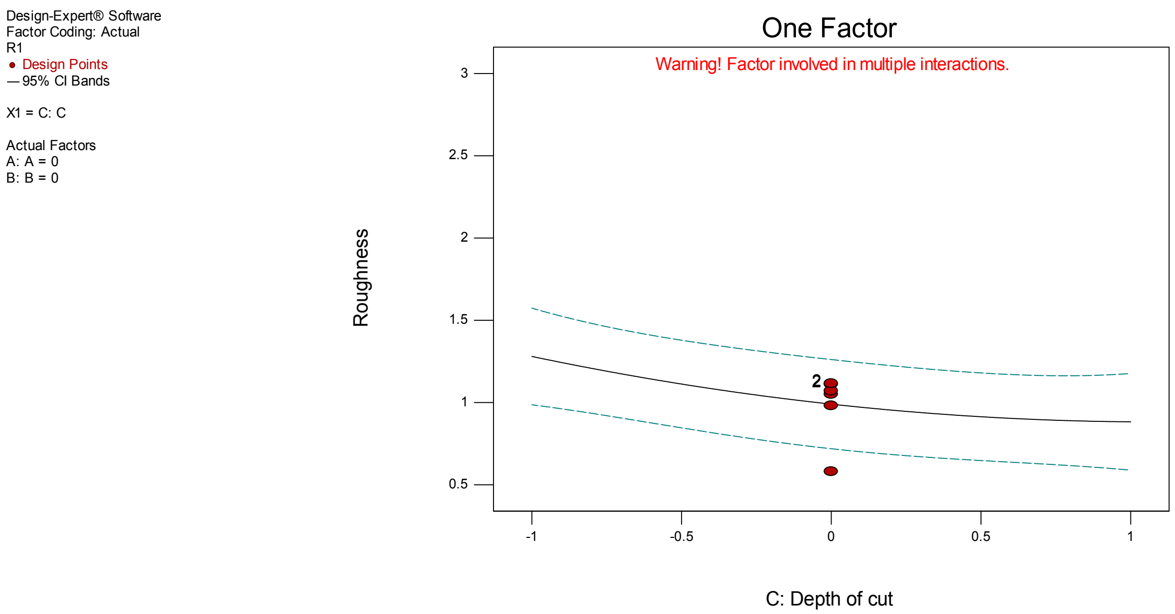


**Figure 7.** Surface Roughness vs Depth of cut.

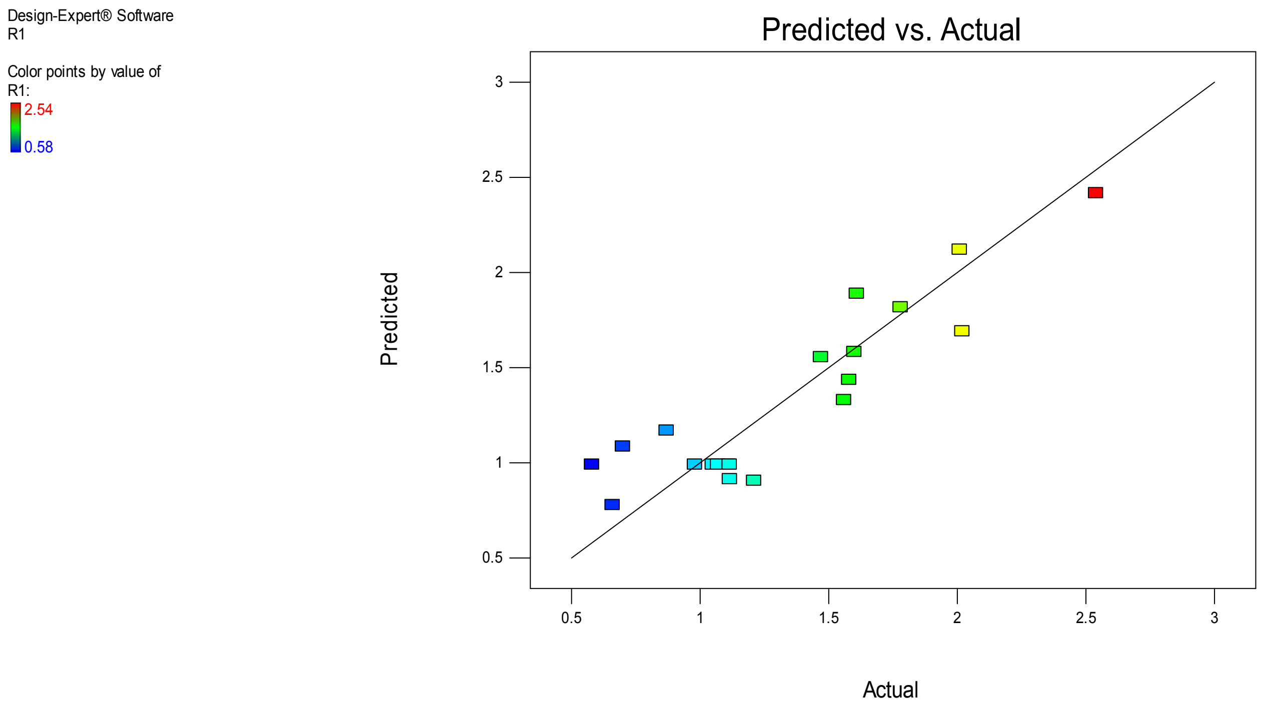


**Figure 8.** Observed vs Predicted

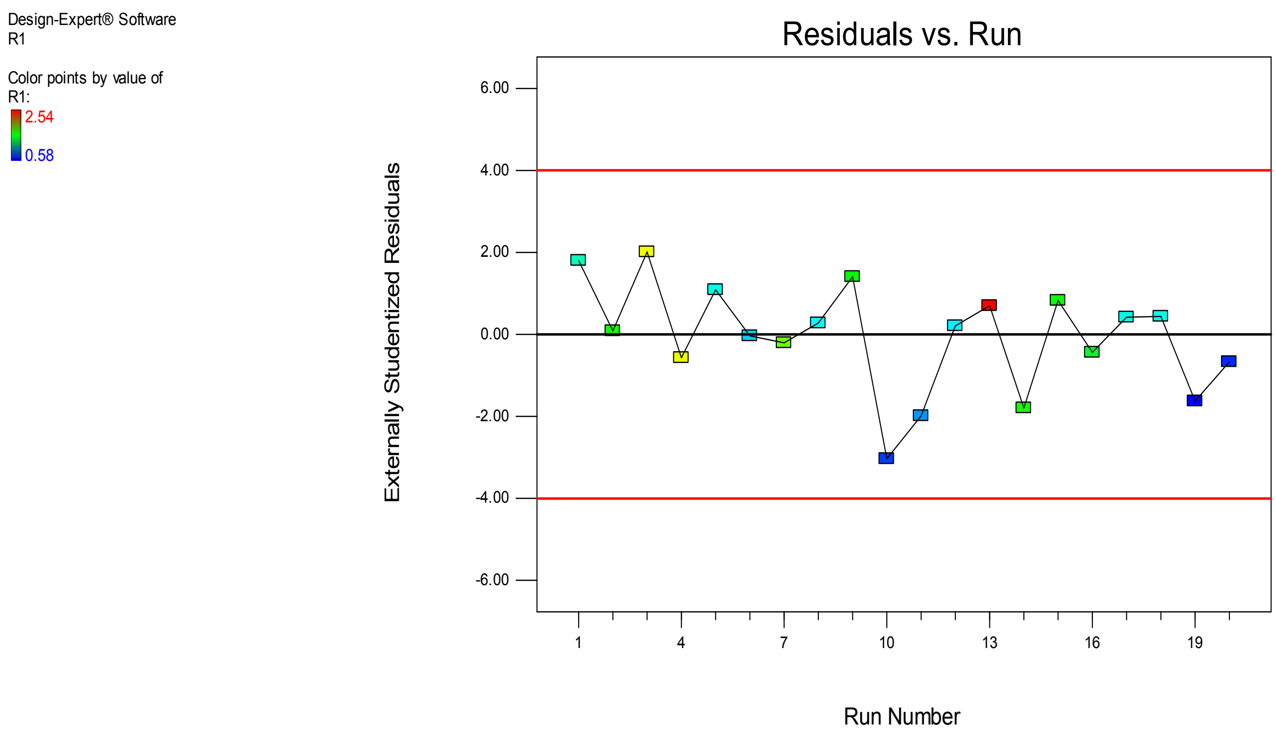


**Figure 9.** Run vs Residuals

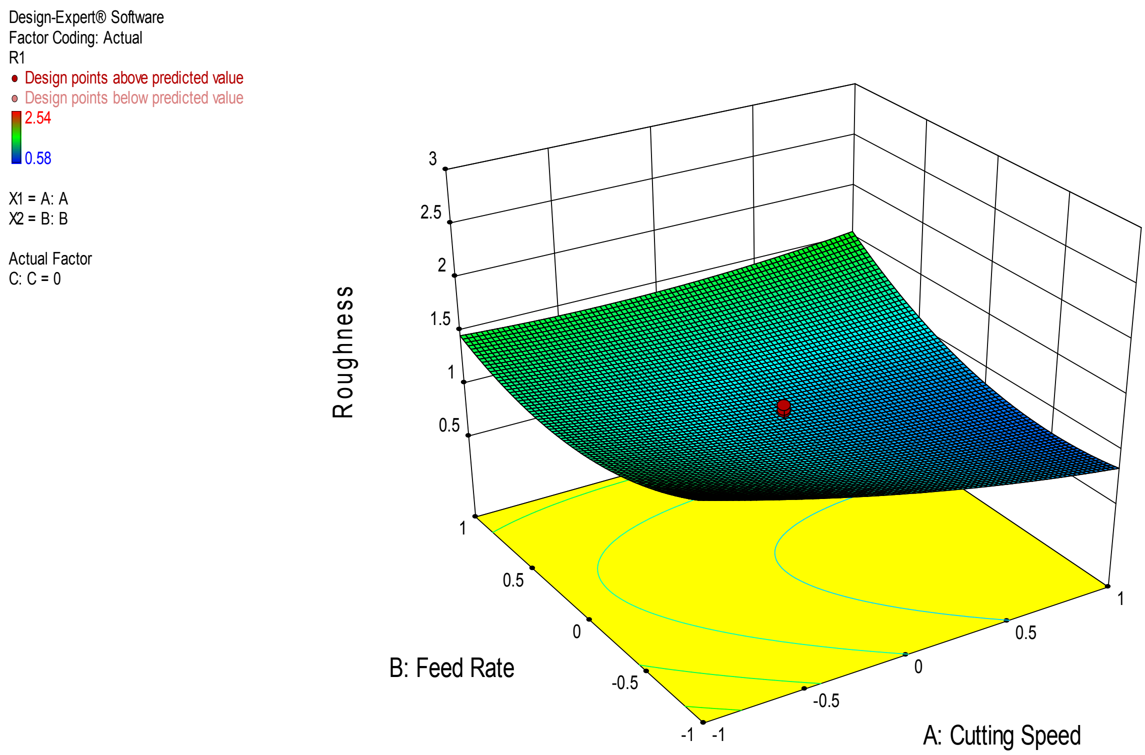


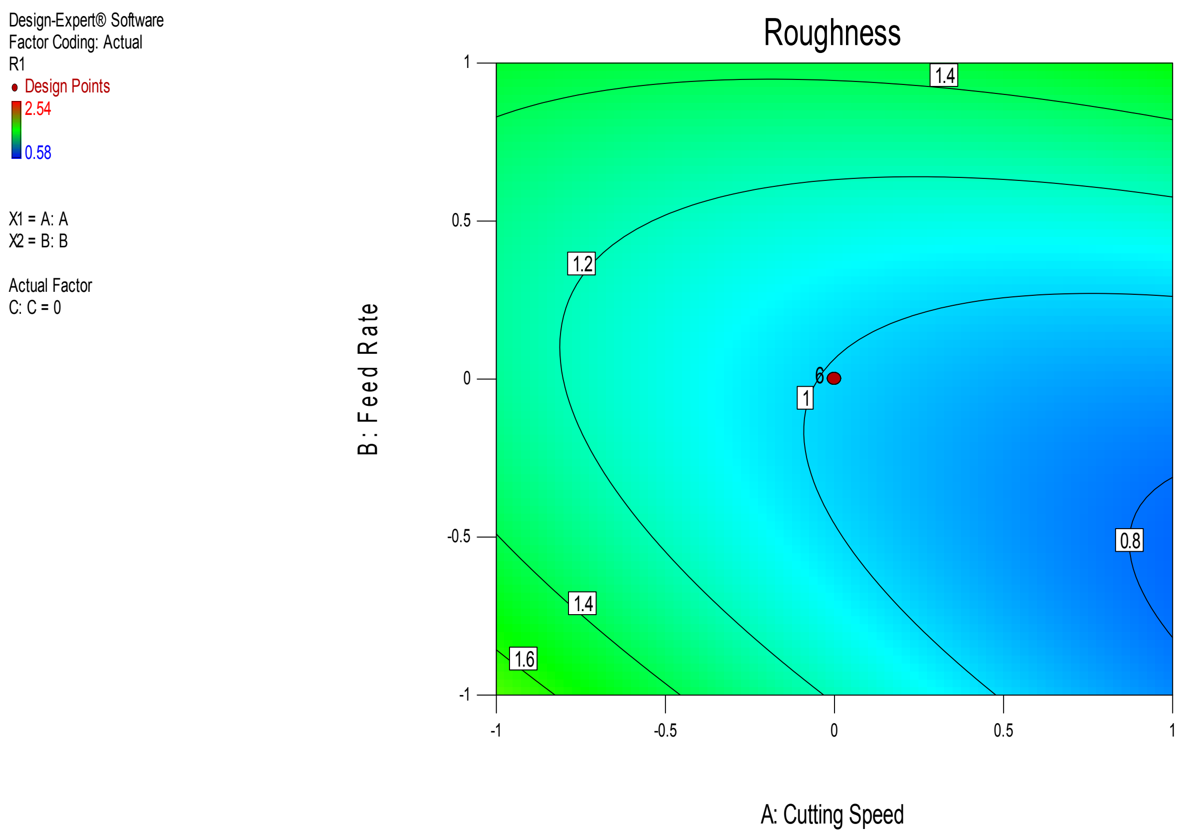


**Figure 10 (a&b).** Contours along with 3D surface for cutting speed and feed rate

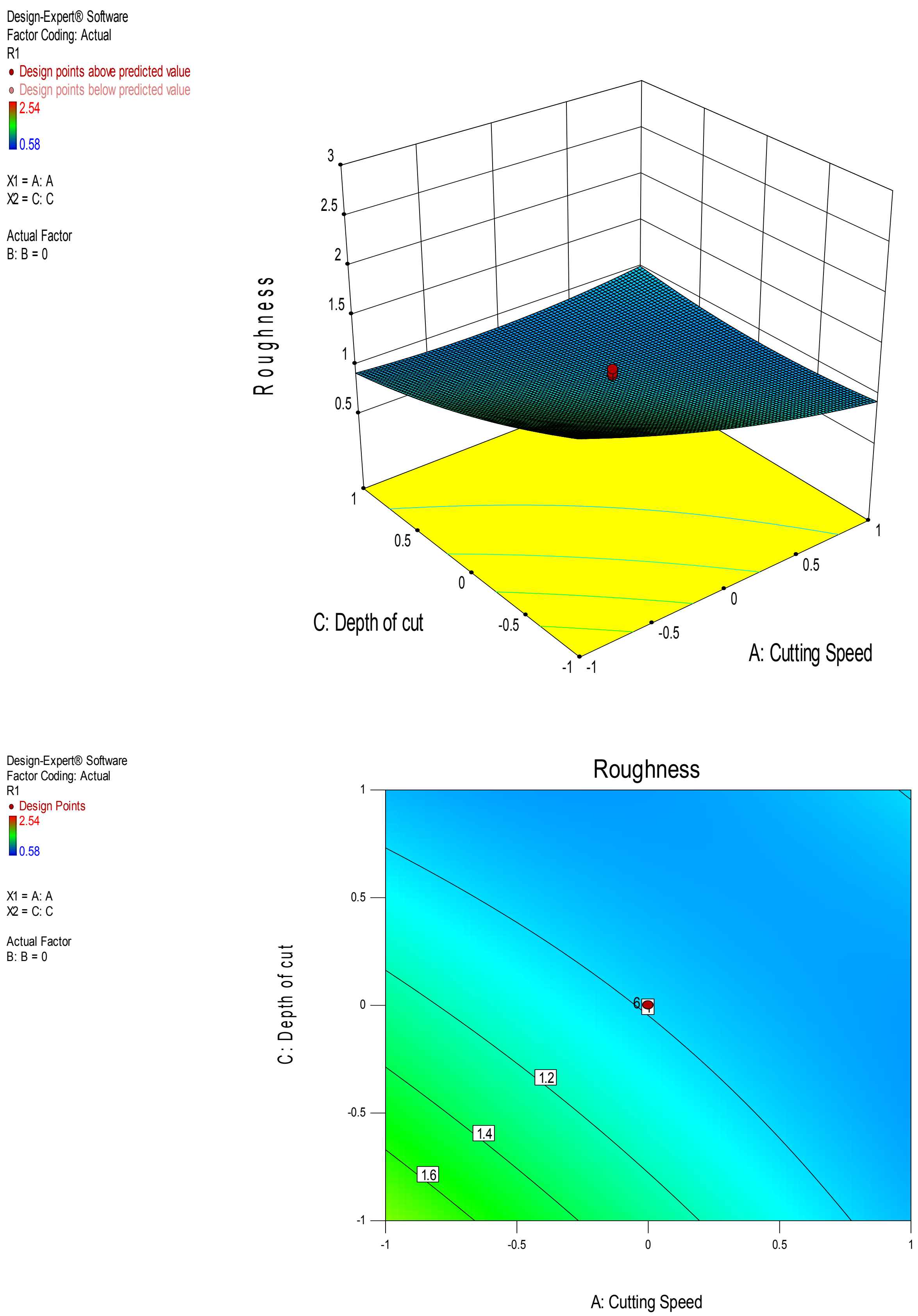


**Figure 11 (a&b).** Contours along with 3D surface for depth of cut and cutting speed

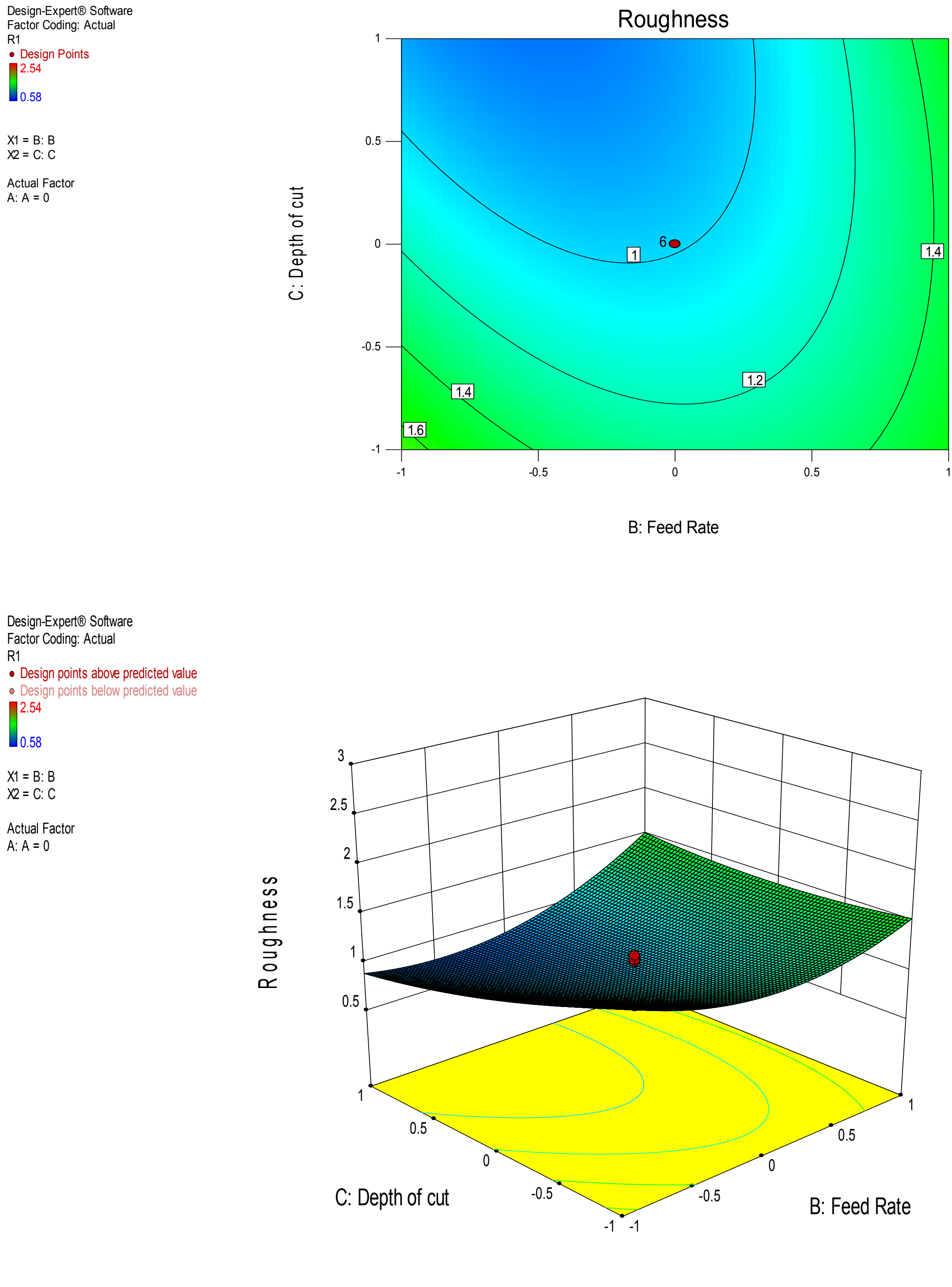


**Figure 12 (a&b).** Contours along with 3D surface for feed rate and depth of cut.

## 3.2 Discussions

### Effect of tool angle on the roughness

Increasing the feed rate and cutting speed increases the cutting temperature [30], which can lead to the softening and burning of the matrix material [31]. Therefore, decreasing the surface roughness for higher feed rates at a high cutting speed might be explained by the adhering of the uncut metallic fibers to the softened matrix under high cutting temperatures.

As it is very well known that cutting forces usually increase with an increase in the feed rate, but the necessity of cutting forces on the cutting speed was found to be varying [32]. It can be understood that as cutting force increases as in the feed rate increases, and there becomes a larger influence on the cutting force for higher cutting speeds. However, the variation of cutting forces remains vary as the cutting speed changes and can be considered in three cutting speed ranges, including (I) low cutting speeds (100-175 m/min), (II) moderate cutting speeds (175-375 m/min), and (III) high cutting speeds (375-500 m/min). In the low cutting speeds, the effect of cutting speed on resultant cutting force is not noteworthy; in the moderate speed, the cutting force increases as with the cutting speed; and whereas in at higher cutting speed, the cutting force weakens as with cutting speed increases. The nonuniform disparity of the cutting force towards cutting speed is steady; as reported by other researchers [31-33]. Since high cutting speed works as a source of temperature so cutting force variation can be correlated to cutting temperatures with the relevance of cutting force. Therefore, at low cutting speeds, it is obvious the of not having comparable cutting temperatures for softening the cutting tool, and hence dry friction predominates. The softening/degrading of the cutting tool in the cutting zone occurs at a critical speed and causes a reduction in cutting forces [32].

In the term of tool angle, one we need the show the effect of the lead angle on the surface roughness which showed nonlinearly variation as with the lead angle and with the cutting speed. The minimum $R_a$ is achievable for a lead angle of 5° for low cutting speeds and 0° for higher cutting speeds, which is revealed the high roughness values for lower cutting speeds as compared to those for higher cutting speeds.

In the terms of rake angle and relief angle, it is observed that surface roughness increases as with the radial rake angle and primary radial relief angle in the general. This may be happened due to the deterioration of tool causing from larger rake angle along with relief angle. At the same time, a radial rake angle also offers an improved surface finish because of easily chip flow [34]. As stated by parallel shear zone concept, larger positive radial rake angle provides higher shear angle [35]. Due to formation of sharp cutting edges on the periphery lateral cutting force extensively reduces. On the other side the excessive rake angle weakens the tool and there becomes chance of acceleration amplitude in feed direction [36]. Consequently, the side surface roughness first decreases and then increases. It is very well known that larger relief angle weakens the friction effect between radial relief surface and side surface of the workpiece due to shortening of the contact length, which causing reduction in adjacent surface roughness with primary radial relief angle [37]. In cutting process, high speed induced cutting temperature causing thermal load is the reason for creating thermal load which induces residual tensile stresses whereas mechanical load caused by cutting force makes the reason for generating residual compressive stress. Consequently, residual compressive stress may increase or decrease with the change in cutting force caused by varying these cutter geometric angles [38]. Accordingly, roughness value may vary.

## 4. Conclusions

This work presented a central composite design approach to study the impact of turning parameters on surface roughness. The following conclusions are drawn from research:

1) Feed rate has the higher effect on the surface roughness. The surface roughness increases very sharply with the increase in feed rate.

2) The surface roughness decreases with the increase in cutting speed and depth of cut has very small effect.

3) Optimal cutting parameters for minimum surface roughness are determined.

4) Closeness between the predicted value and measured showed the adequacy of the developed model for surface roughness on the machining of EN 8.

## References

[1] Sharma, V.S., Dhiman, S., Sehgal, R. and Sharma, S.K., 2008. Assessment and Optimization of cutting Parameters while Turning AISI 52100 Steel. International Journal of Precision Engineering & Manufacturing. 9:54-62.

[2] Fnides, B., Aouici, H. and Yallese, M.A., 2008. Cutting forces and surface roughness in hard turning of hot work steel X38CrMoV5-1 using mixed ceramic. ISSN 1392-1207.

[3] Selvaraj, D.P. and Chandramohan, P., 2010. Optimization of surface roughness of AISI 304 austenitic stainless steel in dry turning operation using Taguchi

design method. Journal of Engineering Science & Technology. 5: 293 - 301.

[4] Kuram, E., Ozcelik, B., Demirbas, E. and Şık, E., June 30 - July 2, 2010. Effects of the Cutting Fluid Types and Cutting Parameters on Surface Roughness and Thrust Force. Proceedings of the World Congress on Engineering Vol. II WCE, London, U.K.

[5] Selvaraj, D.P. and Chandramohan, P., 2010. Influence of cutting speed, feed rate and bulk texture on the surface finish of nitrogen alloyed duplex stainless steels during dry turning. Engineering 2: 453-460.

[6] Hatem, H., 2011. Study the effect of cutting conditions for turning process on the machined surface. Nahrain University, College of Engineering Journal (NUCEJ) 14:61-66.

[7] Sastry, M.N.P., Devi, K.D. and Reddy, K.M., 2012. Analysis and Optimization of Machining Process Parameters Using Design of Experiments. Industrial Engineering Letters. 2:45-50.

[8] Ficici, F., Koksal, S. and Karacadag, M.C., 2012. Optimization of Cutting Parameters for Surface Roughness of Stainless Steel in Drilling Process. International Journal of Advanced Science and Technology 2:13-26.

[9] Korat, M. and Agarwal, N., 2012. Optimization of different machining parameters of En24 alloy steel in CNC turning by use of taguchi method. International Journal of Engineering Research and Applications .2:160-164.

[10] Bhateja, A., Bhardwaj, J., Singh, M. and Pal. S.K., 2013. Optimization of different performance parameters i.e., surface roughness, tool wear rate &SK material removal rate with the selection of various process parameters such as speed rate, feed rate, specimen wear, depth of cut in CNC turning of EN24 alloy steel - an empirical approach. The International Journal of Engineering And Science (IJES). 2:103-113.

[11] Ali, M.H., Khidhir, B.A., Ansari, M.N.M. and Mohamed, B., 2013. FEM to predict the effect of feed rate on surface roughness with cutting force during face milling of titanium alloy. Hbrc Journal 9:263-269.

[12] Vipindas, M.P. and Govindan, P., 2013. Taguchi-Based Optimization of Surface Roughness in CNC Turning Operation. International Journal of Latest Trends in Engineering and Technology. 2:11-20.

[13] Kayastha, C. and Gandhi, J., 2013. Optimization of Process Parameter in Turning of Copper by Combination of Taguchi and Principal Component Analysis Method. International Journal of Scientific and Research Publications. 6:3-12.

[14] Tulasiramarao, B., Srinivas, K., Reddy, P.R., Raveendra, A. and Ravi kumar, B.V.R., 2013. Effect of processing parameters on surface finish of the components processed by CNC turning machine. International Journal of Mechanical Engineering Applications Research 4: 15-18.

[15] Das, S.R., Kumar, A. and Dhupal, D., 2013. Effect of machining parameters on surface roughness in machining of hardened AISI 4340 steel using coated carbide inserts. International Journal of Innovation and Applied Studies. 2:445-453.

[16] Sahijpaul, Y. and Singh, G., 2013. Determining the influence of various cutting parameters on surface roughness during wet CNC turning of AISI 1040 medium carbon steel. Journal of Mechanical and Civil Engineering. 7: 63-72.

[17] Patel, M.T. and Deshpande, V.A., 2014. Optimization of machining parameters for turning different alloy steel using CNC-review. International Journal of Innovative Research in Science, Engineering and Technology. 3:1-5.

[18] Begic-Hajdarevic, D., Cekic, A. and Kulenovic, M., 2014. Experimental study on the high-speed machining of hardened steel. Procedia Engineering. 69: 291-295.

[19] Sarıkaya, M. and Abdulkadir Güllü, A., 2014. Taguchi design and response surface methodology-based analysis of machining parameters in CNC turning under MQL. Journal of Cleaner Production.5:604-616.

[20] Kumar, A., Mahapatra, M.M. and Jha, P.K., 2014. Effect of machining parameters on cutting force and surface roughness of in situ Al-4.5%Cu/TiC metal matrix composites. Measurement 48:325-332.

[21] Baskar, N., Vaiysnavan, R., Prabhu, R. and Prakash, R., 2018. Optimization of machining parameters on EN8 material using Genetic Algorithm. International Journal of Engineering Research & Technology. 6:1-5.

[22] Ren, J., Zhou, J. and Zeng, J., 2016. Analysis and optimization of cutter geometric parameters for surface integrity in milling titanium alloy using a modified grey-taguchi method. Proceedings of the Institution of Mechanical Engineers, Part B: Journal of Engineering Manufacture. 230: 2114-2128.

[23] Pathak, A.D., Warghane, R.S. and Deokar, S.U., 2018. Optimization of cutting parameters in dry turning of AISI A2 tool steel using carbide tool by taguchi based fuzzy logics. Materials Today: Proceedings. 5:5082-5090.

[24] Wang, Z. and Li, L., 2021. Optimization of process parameters for surface roughness and tool wear in milling TC17 alloy using Taguchi with grey relation-

al analysis. Advances in Mechanical Engineering. 13:1-8.

[25] Xiao, M.H., Shen, X.J., Ma, Y., Yang, F., Gao, N., Wei, W.H. and Wu, D., 2018. Prediction of surface roughness and optimization of cutting parameters of stainless steel turning based on RSM. Mathematical Problems in Engineering. 3 :1-15.

[26] Pandey, P.C. and Singh, C.K., 2001. Production Engineering and science; Standard Publishers, Distributors, New Delhi.

[27] Amsted, B.H. and Oswald, P.F., 1996. Manufacturing Processes; Willey Publication.

[28] Yaonan, C., Jinlong, Y., Xinmin, F., and Xu, S., 2018. Experimental study on cutting force and process parameter optimization of plunge milling machining of titanium alloy. Tool Engineering. 52: 65-68.

[29] Bolar, G., Das, A. and Joshi, S.N., 2018. Measurement and analysis of cutting force and product surface quality during end-milling of thin-wall components. Measurement 121: 190-204.

[30] Sreejith, P.S., Krishnamurthy, R., Malhotra, S.K., Narayanasamy, K.J., 2000. Evaluation of PCD tool performance during machining of carbon/phenolic ablative composites. Journal of Materials Processing Technology. 104: 53-58.

[31] Seyedbehzad, G., Jean-François, Ch. and Gilbert, L., 2016. Effect of cutting tool lead angle on machining forces and surface finish of CFRP laminates. Science and Engineering of Composite Materials. 23(5): 543-550.

[32] Sheikh-Ahmad, J.Y., 2008. Machining of Polymer Composites, Springer: New York.

[33] Zhang, L.C., 2009. Cutting composites: A discussion on mechanics modelling. Journal of materials processing technology. 209: 4548-4552.

[34] Subramanian, M., Sakthivel, M. and Sudhakaran, R., 2014. Modelling and analysis of surface roughness of AL7075-T6 in end milling process using response surface methodology. Arabian Journal for Science and Engineering. 39: 7299-7313.

[35] Lalwani, D.I., Mehta, N.K. and Jain, P.K., 2009. Extension of Oxley's predictive machining theory for Johnson and Cook flow stress model. Journal of materials processing technology. 209: 5305-5312.

[36] Subramanian, M., Sakthivel, M., Soorya prakash, K., et al., 2013. Optimization of end mill tool geometry parameters for Al7075-T6 machining operations based on vibration amplitude by response surface methodology. Measurement. 46: 4005-4022.

[37] Buj-Corral, I., Vivancos-Calvet, J. and Gonza lez-Rojas, H., 2011. Influence of feed, eccentricity and helix angle on topography obtained in side milling processes. International Journal of Machine Tools and Manufacture. 51: 889-897.

[38] Migue-lez, M.H., Zaera, R., Molinari, A., Cheriguene, R., Rusinek, A., 2009. Residual stresses in orthogonal cutting of metals: the effect of thermomechanical coupling parameters and of friction. Journal of Thermal Stresses. 32: 269-289.

BILINGUAL PUBLISHING CO.
Pioneer of Global Academics Since 1984

**Journal of Metallic Material Research**
https://ojs.bilpublishing.com/index.php/jmmr

EDITORIAL

# Developing Magnetic Material for Remediation of Aquatic Nitrogen Pollution in Water Facilities

**Guocheng Zhu*** **Junming Chen**

Hunan Provincial Key Laboratory of Shale Gas Resource Utilization, Hunan University of Science and Technology, Xiangtan, Hunan, 411201, China

ARTICLE INFO

*Article history*
Received: December 17, 2021
Accepted: December 18, 2021
Published Online: 24 December 2021

Natural organic matters (NOM) affect water environmental security and have posed a potential threat to human health, and thus they have long been considered as a key index to evaluate water treatment performance. Dissolved organic nitrogen is one of the NOM, which produces some disinfection byproducts having more toxic than those carbon-based materials. Coagulation is a key unit of drinking water purification and has received wide attention. However, conventional flocculation technology on removal of DON is so poor that we have to seek more effective technologies [1,2]. Compared with activated carbon, biological aerated filter and sand filtration, the coagulation efficiency of removing DON is relatively low [3]. The combined use of conventional flocculant and organic polymer can improve treatment efficiency to a certain extent [4,5], and enhanced coagulation can also improve the DON removal rate, but their DON removal performance is still not dreamful [6]. For example, the removal efficiency of DON by conventional water treatment process in China is not good [7]. A drinking water plant in the south of China found that the removal rate of DON in the conventional sewage treatment process (coagulation sedimentation + bio-filter + disinfection) is only 27% [2]; It is reported that among the 28 drinking water plants in the United States, the average removal rate of DON is only 20% [1]. The current flocculation method can only be used to remove particulate matter in raw water, and the effect on removal of those DON with low content, low molecular weight and strong hydrophilicity is not good [8], which still needs to be coupled with relevant processes [3,9,10]. For example,

*Corresponding Author:
Guocheng Zhu,
Hunan Provincial Key Laboratory of Shale Gas Resource Utilization, Hunan University of Science and Technology, Xiangtan, Hunan, 411201, China;
*Email: zhuguoc@hnust.edu.cn*

DOI: https://doi.org/10.30564/jmmr.v4i2.4231

coagulation potassium permanganate [11], coagulation ultrafiltration / microfiltration [9], coagulation adsorption [10], ozone coagulation [12]. These combined processes can improve DON removal rate, but will increase operational process complexity and economic cost. The reason for the poor flocculation is that flocculation usually has a good effect on removal of macromolecules and hydrophobic organics. However, most of the components contained in DON are hydrophilic organics (studies have shown that the proportion of hydrophilic components of DON in the effluent of wastewater treatment plant is as high as 80% [13]. At present, there is a lack of systematic research on flocculation to remove DON. Although some achievements have been made, there is still a big gap between the preparation technology of flocculant and the goal of efficient removal of DON in water.

Magnetic flocculants are often prepared by hybriding nano $Fe_3O_4$ or γ- $Fe_2O_3$ with metal salt flocculants (such as polyaluminium chloride [14], polyferric sulfate [15]) or organic flocculants (such as polyacrylamide (PAM) [16], chitosan [17]. These magnetic flocculants can remove water turbidity, total phosphorus, heavy metals, and algae. However, the effect of those magnetic flocculants prepared using current methods on removing DON is still not ideal. Often, after flocculation, under the action of magnetic field, the flocculation sedimentation speed is fast, but the DON removal efficiency is not improved. Too high dosage will also lead to poor flocculation result. The main reason for the poor magnetic flocculation effect may be that the adsorption performance of magnetic nanoparticles is closely related to the microstructure of magnetic nanoparticles (such as particle size, specific surface area, surface functional groups), environmental conditions (such as temperature, pH value, ion type and strength) [18,19]. Magnetic nanoparticles (MNPs) modified by cyclodextrin have good adsorption effects on amino acids, phenylalanine and tyrosine [20]. For treatment of secondary effluent of industrial wastewater, some studies show that the use of $Fe_3O_4$ mainly has the effect of accelerating separation, but the adsorption effect is not good. However, with the synergistic flocculation of amino functionalized $Fe_3O_4$ it has a good effect on removing water protein, polysaccharide and humic acid, which can meet the water quality discharge standard and reduce the dosage of flocculant [21]. The above results show that functional nanoparticle materials are of great significance to improve the adsorption and flocculation performance. Therefore, the functional modification of magnetic nanoparticles plays an important role.

The surface modification of magnetic nanoparticles is diverse, and a variety of modifiers can be introduced into the surface. Although different groups will be introduced into $Fe_3O_4$ modified by organic substances such as chitosan and polyacrylamide, the effect of chitosan and polyacrylamide on the removal of DON is not good. After compounding with magnetic nanoparticles, the effect of improving the removal of DON is also limited. Therefore, how to increase the site-specific selection and adsorption capacity is an important problem to improve the pollutant removal efficiency of magnetic nanoparticles and magnetic flocculant. The removal of micro pollutants in water has always been a difficult problem in some water treatment methods [22], such as flocculation and activated carbon adsorption. It is found that some porous materials have good removal effect on such pollutants after modification, such as porous materials β-Cyclodextrin [22], porous aluminum Pillared Bentonite [23] (good adsorption of DON in water). The adsorption effect of these materials is closely related to the structure of adsorption materials. Compared with these porous materials, metal organic frameworks (MOFs) materials have the advantages in specific surface area, porosity and convenience in synthesis [24].

The surface modification of magnetic nanoparticles is diverse, and a variety of modifiers can be introduced into its surface. Although $Fe_3O_4$ modified by organic compounds such as chitosan and polyacrylamide will introduce different groups, the removal effect of chitosan and polyacrylamide on DON is not ideal. After being coupled with magnetic nanoparticles, the effect of improving DON is also limited. Therefore, how to improve site selection and adsorption capacity of magnetic nanoparticles is a key point. In some water treatment methods, the removal of trace pollutants in water has always been a difficult problem [22], such as flocculation and activated carbon adsorption. It is found that the modified porous materials have a good removal effect on such pollutants, such as porous materials β- Cyclodextrin [22], porous aluminum Pillared Bentonite [23] (good adsorption of DON). The adsorption effect of these materials is closely related to the structure of adsorbents. Compared with these porous materials, metal organic frameworks (MOFs) materials have advantages in specific surface area, porosity and convenient synthesis [24].

The MOFs have the advantages of easy functional modification, easy structure adjustment and various adsorption mechanism, and the functional group modified MOFs have higher selectivity, and can obtain better properties after compounding with other functional materials [25]. At present, the research on MOFs for drinking water treatment has been reported [26]. Combining the magnetism of magnetic nanoparticles with the porous structure of MOFs can obtain easily separated, easily dispersed and reusable magnetic MOFs composites [27]. It can not only retain the structure and properties of MOFs materials, but also increase the magnetism of nanoparticles. Through the regulation of synthesis conditions, magnetic MOFs materials for specific applications have been applied in the field of water treatment [28]. At present, magnetic MOFs are widely studied in the removal of gas pollutants, but there are relatively few studies on the removal of water pollutants. Therefore, application of MOFs in the field of water environment analysis and remediation needs to be further developed [25].

MOF has advantages of easy functional modification, easy structural adjustment and varied adsorption mechanism. Functional groups modified MOF has higher selectivity and can obtain better properties after hybriding with other functional materials [25]. Application of MOF in drinking water treatment has been reported [26]. Combining magnetic nanoparticles with MOFs forms magnetic MOFs composites are easier to make MOFs disperse and reusable [27]. It can not only maintain the structure and properties of MOFs materials, but also improve the magnetism of the materials. Through adjusting the synthesis conditions, magnetic MOFs materials have been applied in specific field of water treatment [28]. At present, magnetic MOF has been widely studied in the removal of gas pollutants, but less used in the removal of water pollutants. Therefore, the application of MOF in the field of water environment analysis and remediation needs to be further developed [25].

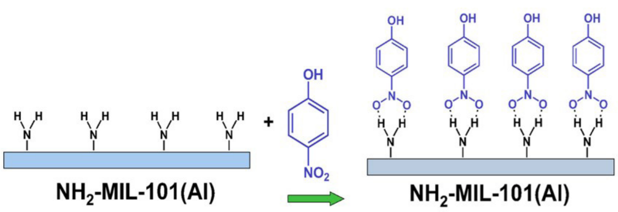


**Figure 1.** Adsorption mechanism diagram of nitrophenol onto $NH_2$-MIL-101(Al) [30]

The results show that MOFs can interact with nitrogen-containing organic compounds through π - π bonds and hydrogen bonds. For example, MOF can adsorb nitrogen-containing compounds through π - π bonds: CuCl/MIL-100 (CR) adsorbs nitrogen-containing compounds in fuel [29]; MOF adsorbs nitrogen-containing organic compounds through hydrogen bonding [30], such as nitrophenol adsorbed by $NH_2$-MIL-101 (Al) (see Figure 1). Although there are different environments and types of organic nitrogen compounds, the removal of DON by MOFs modified nanoparticles hybridized coagulant would be a promising method.

## References

[1] Lee, W., Westerhoff, P., 2006. Dissolved organic nitrogen removal during water treatment by aluminum sulfate and cationic polymer coagulation. Water Research. 40(20), 3767-3774.

[2] Liu, B., Gu, L., Yu, X., Zhang, H.N., 2012. Dissolved organic nitrogen (DON) in a full-scale drinking water treatment plant. Aqua 61(1), 41.

[3] Pramanik, B.K., Choo, K.H., Pramanik, S.K., Suja, F., Jegatheesan, V., 2015. Comparisons between biological filtration and coagulation processes for the removal of dissolved organic nitrogen and disinfection by-products precursors. International Biodeterioration & Biodegradation. 104, 164-169.

[4] Lee, W., Westerhoff, P., 2006. Dissolved organic nitrogen removal during water treatment by aluminum sulfate and cationic polymer coagulation. Water Res. 40(20), 3767-74.

[5] Zhang, H.N., Gu, L., Yu, X., 2011. Effect of chemical pre oxidation on removal of dissolved organic nitrogen in water by coagulation. Abstracts of the 6th National Conference on Environmental Chemistry and exhibition of environmental scientific instruments and analytical instruments.

[6] Gustafson, R.B., 2012. Evaluation of enhanced coagulation for the removal of dissolved organic nitrogen and the control of nitrogenous disinfection byproduct formation. Dissertations & Theses - Gradworks.

[7] Gu, L., Liu, B., Yu, X., 2010. Organic nitrogen compounds in drinking water treatment process of polluted water source. Scientific Bulletin. 55(26), 2651-2654.

[8] Matilainen, A., Vepsalainen, M., Sillanpaa, M., 2010. Natural organic matter removal by coagulation during drinking water treatment: a review. Adv Colloid Interface Sci. 159(2), 189-97.

[9] Arnaldos, M., Pagilla, K., 2010. Effluent dissolved organic nitrogen and dissolved phosphorus removal by enhanced coagulation and microfiltration. Water Research. 44(18), 5306-5315.

[10] Liu, B., Yu, G.Z., Gu, L., Zhao, C.M., Li, Q.F., Zhai, H.M., 2013. Removal of DON in Micro-polluted Raw Water by Coagulation and Adsorption Using Activated Carbon. Environmental Science. 34(4), 1392-1401.

[11] Liu, C., He, S., Wang, B., Wang, J., Chen, W., 2016. Enhanced performance and mechanism of KMnO4 pre-oxidation to coagulation on the removal of the DON and proteins. Water Science & Technology Water Supply. 16(5), 1432-1440.

[12] De Velásquez Orta, M.T., 2010. Ozone application during coagulation of wastewater: effect on dissolved organic matter. Ozone Science & Engineering. 32(5), 323-328.

[13] Liu, H., 2012. Algal uptake of hydrophobic and hydrophilic dissolved organic nitrogen in effluent from biological nutrient removal municipal wastewater treatment systems. Environmental Science & Technology. 46(2), 713-721.

[14] Zhang, M., Xiao, F., Wang, D.Sh., Xu, X.Zh., Zhou, Q., 2017. Comparison of novel magnetic polyaluminum chlorides involved coagulation with traditional magnetic seeding coagulation: Coagulant characteristics, treating effects, magnetic sedimentation efficiency and floc properties. Separation & Purification Technology. 182, 118-127.

[15] Jiang, Ch., Wang, R., Ma, W., 2010. The effect of magnetic nanoparticles on Microcystis aeruginosa removal by a composite coagulant. Colloids & Surfaces A Physicochemical & Engineering Aspects. 369(1-3), 260-267.

[16] Zhou, Z., Shan, A., Zhao, Y., 2017. Synthesis of a novel magnetic polyacrylamide coagulant and its application in wastewater purification. Water Science & Technology. 75(3), 581-586.

[17] Liu, B., Chen, X., Zheng, H., Wang, Y., Sun, Y., Zhao, C., Zhang, S., 2018. Rapid and efficient removal of heavy metal and cationic dye by carboxylate-rich magnetic chitosan flocculants: Role of ionic groups. Carbohydrate Polymers. 181, 327.

[18] Mohammed, L., Gomaa, H.G., Ragab, D., Zhu, J., 2017. Magnetic nanoparticles for environmental and biomedical applications: A review. Particuology. 30(1), 1-14.

[19] Yang, B.J., 2012. Preparation of ferroferric oxide particles by solvent-thermal method and preparation of magnetite-composite particles. Lanzhou University.

[20] Kakhki, R.M., 2015. Application of magnetic nanoparticles modified with cyclodextrins as efficient adsorbents in separation systems. Journal of Inclusion Phenomena & Macrocyclic Chemistry. 82(3-4), 301-310.

[21] Ren, H.Q., Chu, X., Ding, L.L., Tao, Y.Ch., 2016. A new magnetic nano magnetic seed and its method and application for treating industrial biochemical tail water, Chinese patent.

[22] Alsbaiee. A., Smith, B.J., Xiao, L.L., Ling, Y.H., Helbling, D.E., Dichtel, W.R., 2016. Rapid removal of organic micropollutants from water by a porous β-cyclodextrin polymer. Nature 529(7585), 190-194.

[23] Yang, Zh., Shang, Y.B., Lu, Y.B., Chen, Y.Ch., Huang, X., Chen, A.M., Jiang, Y.X., Gu, W., Qian, X.Zh., Yang, H., Cheng, R.Sh., 2011. Flocculation properties of biodegradable amphoteric chitosan-based flocculants. Chemical Engineering Journal. 172(1), 287-295.

[24] Zhang, H., Li, G.L., Zhang, K.G., Liao, Ch.Y., 2017. Advances of Metal-Organic Frameworks in Adsorption and Separation Applications. Journal of Chemistry. 75(9), 841-859.

[25] Huo, J.B., Cui, H.J., Fu, M.L., Yuan, B.L., 2017. The fabrication of magnetic metal-organic frameworks composites and their application in environment. Scientia Sinica (Chimica). 47(7), 830-843.

[26] Feng, D., Wei, C.X., Xia, Y., 2017. Progress in the applications of functionalized metal-organic frameworks for adsorption and removal of pollutants in drinking water. Chinese Journal of Chromatography. 35(3), 237-244.

[27] Fu, Y.Y., Yan, X.P., 2013. Metal-Organic Framework Composites. Progress in Chemistry. 25(203), 221-232.

[28] Shi, Z.N., Xu, Ch., Guan, H., Li, L., Fan, L., Wang, Y.X., Liu, L., Meng, Q.T., Zhang, R., 2017. Magnetic Metal Organic Frameworks (MOFs) Composite for Removal of Lead and Malachite Green in Wastewater. Colloids & Surfaces A Physicochemical & Engineering Aspects.

[29] Ahmed, I., Jhung, S.H., 2014. Adsorptive denitrogenation of model fuel with CuCl-loaded metal-organic frameworks (MOFs). Chemical Engineering Journal. 251(251), 35-42.

[30] Liu, B.J., Yang, F., Zou, Y.X., Peng, Y., 2014. Adsorption of Phenol and p-Nitrophenol from Aqueous Solutions on Metal-Organic Frameworks: Effect of Hydrogen Bonding. Journal of Chemical & Engineering Data. 59(5), 1476-1482.

# *Journal of Metallic Material Research*

## *Aims and Scope*

***Journal of Metallic Material Research*** is a peer-reviewed, open-access journal dedicated to the research of metallic materials. As a critical component of the human civilization, metal has been infused into many aspects of our lives. The journal is focused on innovations in the research of metallic materials.

The scope of the Journal of Metallic Material Research includes, but is not limited to:

- Properties of metallic materials (Physical/Mechanical/Electrical/Chemical)
- Functions of metallic materials
- Applications of metallic materials
- Alloys
- Recycling

**Bilingual Publishing Co. (BPC)**

Tel:+65 65881289

E-mail:contact@bilpublishing.com

Website:www.bilpublishing.com

## About the Publisher

Bilingual Publishing Co. (BPC) is an international publisher of online, open access and scholarly peer-reviewed journals covering a wide range of academic disciplines including science, technology, medicine, engineering, education and social science. Reflecting the latest research from a broad sweep of subjects, our content is accessible worldwide——both in print and online.

BPC aims to provide an analytics as well as platform for information exchange and discussion that help organizations and professionals in advancing society for the betterment of mankind. BPC hopes to be indexed by well-known databases in order to expand its reach to the science community, and eventually grow to be a reputable publisher recognized by scholars and researchers around the world.

BPC adopts the Open Journal Systems, see on ojs.bilpublishing.com

# Database Inclusion

Asia & Pacific Science Citation Index

Creative Commons

China National Knowledge Infrastructure

Google Scholar

Crossref

MyScienceWork

BILINGUAL
PUBLISHING CO.
Pioneer of Global Academics Since 1984

Tel:+65 65881289
E-mail: contact@bilpublishing.com
Website:ojs.bilpublishing.com

2630-5135
02
9 772630 513212